Efficient, Scalable, and Accurate Localization with Ultra-wideband Radios Through Concurrent Transmissions

by

Milad Heydariaan

A dissertation submitted to the Department of Computer Science,

College of Natural Sciences and Mathematics

in partial fulfillment of the requirements for the degree of

Doctor of Philosophy
in Computer Science

Chair of Committee: Omprakash Gnawali

Committee Member: Jaspal Subhlok

Committee Member: Edgar Gabriel

Committee Member: Kyungki Kim

University of Houston
May 2020

ACKNOWLEDGMENTS

I wish to express my deepest gratitude to my Ph.D. advisor, Prof. Omprakash Gnawali, for all his help and support during my Ph.D. study, my research, and writing this dissertation. He has guided me through my Ph.D. study with his enthusiasm, motivation, patience, and kindness. I am forever indebted to him not only for helping me to learn the necessary Ph.D. skills but also for helping me to learn how to become a better person.

I would like to extend my gratitude to other committee members of this dissertation, Prof. Jaspal Subhlok, Prof. Edgar Gabriel, and Prof. Kyungki Kim, for their insight, guidance, and support on my work.

I would like to express my sincere gratitude to my supervisors and colleagues at Robert Bosch Research and Technology Center, Dr. Martin Coors, Dr. Vivek Jain, Dr. Maurizio Bocca, and Dr. Wei Mao, Dr. Sushanta Rakshit, and Dr. Yakup Kilic for their guidance and encouragements during my several internships. I am grateful to Dr. Martin Coors for everything he has taught me, his support, and patience. Martin has remarkable helped me to push myself and discover my capabilities.

I would like to thank my colleagues at the Networked Systems Laboratory, Hessam Mohammadmoradi, Shengrong Yin, Dong Han, Qiang Li, Nour Smaoui, Nacer Khalil, and Alireza Ansaripour, for their collaborations and fruitful discussions. I am deeply grateful to Hessam Mohammadmoradi, who stood by my side like a brother through all the tough times during my Ph.D. study.

I would like to thank my other collaborators and friends at the University of Houston, Hosein Neeli, Taha Eghtesad, Millad Ghane, Hossein Dabirian, and Yaser Karbaschi. I am genuinely thankful to Hosein Neeli for his encouragement and restless efforts in helping me to carry out experiments on several occasions.

My deepest gratitude goes to my beloved family. I could not have completed my Ph.D. and this dissertation without the unconditional love and support of my father, Abbas, my mother, Firouzeh, my brother, Mehrdad, and my wife, Sheyda. I am eternally thankful to my lovely and beautiful wife for always believing in me and being there for me through the stressful and challenging times in the journey to finish my Ph.D. study.

PREVIOUSLY PUBLISHED MATERIAL

Chapter 4 revises a previous publication [26]:

M. Heydariaan, H. Mohammadmoradi, O. Gnawali.

Toward Standard Non-line-of-sight Benchmarking of Ultra-wideband Radio-based Localization,

Proc. IEEE CPSBench, 2018.

Chapter 5 revises a previous publication [27]:

M. Heydariaan, H. Mohammadmoradi, O. Gnawali.

R3: Reflection Resilient Concurrent Ranging with Ultra-Wideband Radios,

Proc. IEEE DCOSS, 2019.

Chapter 6 revises a previous publication [25]:

M. Heydariaan, H. Dabirian, O. Gnawali.

AnguLoc: Concurrent Angle of Arrival Estimation for Indoor Localization with UWB Radios,

Proc. IEEE DCOSS, 2020.

ABSTRACT

The technology to determine the location of a mobile device, also called localization technology, enables us to develop applications and systems that can optimize our work and lives in the physical world. Many IoT applications today rely on GPS for localization. However, GPS fails to provide the necessary location accuracy for indoor applications. Ultra-wideband (UWB) radios have facilitated accurate and precise (10 cm) indoor localization in the past few years. Wireless interference can severely impact the performance of localization and communication systems. Many localization and communication systems avoid or mitigate the destructive interference, which can lead to inefficient use of the wireless spectrum. A relatively new research approach to increase efficiency and scalability is to enable concurrent transmissions, i.e., create techniques that allow multiple transmitters to transmit their packets concurrently while enabling the receivers to successfully receive and decode those packets and consequently reduce the total time required for packet exchanges. Time-of-arrival (ToA)-based localization and angle-of-arrival (AoA)-based localization are two common techniques for precise indoor localization with UWB radios. A UWB receiver node can measure the difference in ToA or AoA from multiple UWB transmitter nodes by analyzing the channel impulse response (CIR). Related work investigated the feasibility of UWB ToA-based concurrent localization, but existing solutions are not practical in real-world environments due to scalability and accuracy issues. To the best of our knowledge, there is no prior work on concurrent AoA estimation. In this dissertation, we focus on three main challenges: (1) designing a reflection resilient concurrent response detection algorithm by making use of the difference between the time deviation of concurrent peaks and multipath components (MPCs); (2) relaxing transmitter processing time constraints by using a clock skew correction method to minimize inaccuracies caused by clock drift; and (3) investigating the feasibility of concurrent AoA estimation with UWB radios and designing an efficient, scalable, and accurate indoor localization system using the angle difference of arrival (ADoA) technique. Our research not only creates new algorithms and designs of localization systems but also evaluates their performance using real-world implementations on state-of-the-art hardware platforms and testbeds.

TABLE OF CONTENTS

LIST OF TABLES

LIST OF FIGURES

Chapter 1

Introduction

Finding the location of persons and things has always been of interest to people. Humanity has always been looking for efficient and effective ways to accomplish their goals of locating people and things. Applications of localization, such as tracking and navigation, can help us in numerous ways in our everyday lives. For example, navigation is more efficient if we know our current location on a map and possible paths to the destination. Asset tracking, safety, proximity marketing, and warehouse monitoring are some of important applications of location tracking. Location-based services (LBS) have become an essential component of the Internet of Things (IoT) in the past few years. Knowing the location of sensors and mobile devices helps us infer useful information and insights about our surroundings. We can use the Global Positioning System (GPS), Galileo, or Global Navigation Satellite System (GLONASS) to find the current location of IoT devices. However, in indoor environments, these positioning systems fail to provide the accuracy and precision level required by many indoor applications, since the direct path or the line-of-sight is blocked by building structures. With the development of ultra-wideband (UWB) radios, it is possible for indoor localization systems to achieve highly accurate and precise (10 cm) position estimation [10]. UWB radios utilize a bandwidth larger than 500 MHz, which makes them resilient to multipath fading effect. Compared to narrow-band and wide-band, these radios have a better ability to detect first path, or line of sight (LoS), and consequently better performance when it comes to calculating the time of arrival (ToA) of a packet.

We investigated problems in UWB-based localization systems and identified two main challenges. First, in case of completely blocked LoS or presence of strong multipath, non-line of sight (NLoS) signals can degrade the performance of ToA estimation and decrease the accuracy of location estimates. In most realistic environments, NLoS is inevitable. Numerous research studies already investigated the problem of NLoS [13, 24, 32]. In our work, we examine the NLoS problem by carefully looking at the behavior of radio frequencies (RF) and their impact on UWB indoor localization. Second, like many other wireless technologies, UWB radios are prone to failure in the presence of destructive interference. The interference is inevitable when multiple wireless devices use the same part of the wireless spectrum at the same time for communication. Researchers studied the impact of wireless interference on the performance of UWB localization [48]. When we look at the above two problems in the context of scalability, the main challenge is wireless interference. According to IoT Analytics, the number of connected IoT devices reached 7 billion in 2018. This number is forecast to reach 21.5 billion by 2025 [39]. It is crucial to find scalable and efficient solutions to tackle the interference issue.

1.1 Scalability and Efficiency of UWB-based Indoor Localization Systems

There is a body of research in the area of wireless communications that address the problem of wireless interference. Traditional solutions suggest using medium access control (MAC) protocols to either avoid/prevent or mitigate the destructive interference. Since carrier sensing is generally not feasible for UWB radios, IEEE 802.15.4 UWB standard suggests using ALOHA protocol as the UWB MAC protocol [30]. ALOHA and similar MAC protocols are not scalable. These solutions are only suitable for networks with a low density of channel access since their performance drops drastically beyond 18% channel utilization [11, 38]. In fact, finding a scalable MAC protocol for UWB networks is still an open problem.

In traditional localization solutions, there is a trade-off between scalability and efficiency. To support a large number of devices, these solutions avoid or mitigate interference, leading to inefficient use of the wireless spectrum. Some solutions separate the transmission (TX) time of each device by using a time-division multiple access (TDMA) method or a random access/back-off protocol. We call these techniques the class of *avoiding interference*. Avoiding interference usually impairs the ability of a system to scale. Solutions that avoid interference only allow one device to transmit (TX) at a time. With an increase in the number of devices, it becomes harder to avoid interference while maintaining a fast update rate for all nodes. Another category of solutions removes or minimizes the impact of interference by correcting the errors in the received (RX) signals and packets. We call these techniques the class of *mitigating interference*. Mitigating interference decreases efficiency. Solutions that mitigate interference make use of additional information embedded in the packet to recover from errors or use redundant packets to increase the chance of transmission without interference. With the increase in the level of interference, mitigation of interference incurs a large overhead.

A more promising solution to tackle the interference problem is to utilize concurrent transmissions. Concurrency-based solutions allow signals from multiple transmitters (TX) to overlap. Traditional localization and communication systems utilize concurrent transmission to increase the probability of packet reception (RX) [18, 32]. When multiple devices transmit the same packet at the same time, constructive interference increases the received signal power; hence, the receiver (RX) has a higher chance to decode the packet correctly. A number of recent studies in the area of UWB radios utilize concurrent transmissions differently, aiming to increase the scalability and efficiency of localization systems [6, 7, 22, 23]. Concurrency-based UWB localization systems allow signals from multiple devices to overlap to reduce the time required for all transmissions to finish. These solutions exploit features of the channel impulse response (CIR) of overlapping packets to extract information about each transmitter.

In concurrency-based UWB localization systems, an initiator node broadcasts a *SYNC* packet to synchronize multiple responder nodes. Upon reception of the *SYNC* packet, responder nodes schedule their next transmission in a way that they almost completely overlap. The estimated CIR at the receiver contains information about each transmitter. The receiver can extract information about the physical placement of each responder by analyzing signal peaks in the CIR. A peak in the CIR indicates the arrival of a signal belonging to a responder node. Many of the indoor localization systems, including state of the art [7,23], have been demonstrated on the DW1000 [10] UWB radio platform. DW1000 accurately estimates the time of arrival (ToA) of the first arriving signal (first path). DW1000 uses a threshold to separate the channel noise from the first path. In concurrency-based localization systems, a receiver can emulate the same algorithm used by DW1000 to detect signals from other responders. Further, the receiver can calculate the difference between the ToA of the first responder and other responders. Concurrency-based UWB localization solutions use the difference in ToA to find the location of the receiver tag node. However, these solutions face three challenges that affect their localization accuracy and their ability to scale:

1. **Strong multipath**: Concurrency-based UWB localization solutions rely on detecting signal peaks from multiple responder nodes in the CIR estimate at the receiver. In the presence of strong multipath, it is hard to distinguish responder signal peaks from multipath components (MPCs). To tackle this issue, the state of the art suggests response delay modulation, which is separating responder signal peaks by adding a specific delay to each response [7,23]. The amplitude of MPCs decreases when they get farther away than the first responder peak. With enough separation, we can assume that the amplitude of any MPCs would be negligible compared to the responder peak. However, this solution impacts the scalability of responders since CIR has limited space.

2. **Clock drift**: Responder nodes usually use separate free-running oscillators. The behavior of each oscillator depends on its mechanical characteristics and environmental effects such as temperature, voltage, vibration, pressure, etc. The different behavior of each oscillator causes clock drift against each other. Clock drift causes inaccuracies in packet transmission scheduling, which ultimately impacts the accuracy of the ToA estimate of multiple responder

peaks. The literature in this area suggests minimizing the processing and scheduling delay at the responder nodes to minimize the effect of clock drift [6,7]. This solution increases the complexity and makes it hard to implement such systems in real-world scenarios.

3. **Transmission scheduling uncertainty**: The transmission scheduling uncertainty of DW1000 introduces a jitter of approximately 8 ns, which can cause up to 2.4 m of the localization error. Solutions provided by state of the art require the transmission of additional information to tag receiver nodes and the knowledge of antenna delays to correct the error induced by this scheduling uncertainty [23]. These solutions increase the complexity of such systems and make them harder to deploy and implement in real-world scenarios.

1.2 Dissertation Contributions

In this dissertation, we address all three issues mentioned above. We also take the initial steps in standardizing NLoS benchmarking to make results from different studies comparable. We make the following contributions:

- We study the feasibility of providing a standard benchmarking framework to compare results from different studies that build UWB-based localization solutions. We present a methodology to observe the effects of attenuation and refraction on UWB radio signals by minimizing reflection and diffraction. We explore the true effect of attenuation and refraction on UWB radio signals when the signal propagates in different construction materials. We published this work as a workshop paper at IEEE CPSBench 2018.

- We study the feasibility of detecting concurrent peaks from MPCs. We design an algorithm to detect concurrent responses in run-time, resilient to strong reflections. Our algorithm makes use of the difference between the time deviation of concurrent peaks and multipath components (MPCs). Further, we relax responder processing time constraints by using a clock skew correction method to minimize inaccuracies caused by clock drift. We published this work as a conference paper at IEEE DCOSS 2019.

- We study the feasibility of providing a solution to increase the accuracy of concurrent localization systems. For this purpose, we study the feasibility of concurrent angle of arrival (AoA) estimation with UWB radios and comparison with sequential AoA estimation baseline. Since AoA estimation only relies on the phase difference of arrival (PDoA) between multiple antennas at a receiver, it is unaffected by the transmission scheduling uncertainties. Further, we design an efficient, scalable, and accurate indoor localization system using the angle difference of arrival (ADoA) technique. Our algorithm works with both sequential AoA and concurrent AoA, overcomes the front-back angle measurement ambiguity problem, and works with unknown tag tilting. We published this work as a conference paper at IEEE DCOSS 2020.

In summary, despite the efforts in improving the scalability and efficiency of UWB-based localization systems, there are still many challenges and issues left unaddressed, which affect their accuracy, scalability, and implementability in the real-world scenarios. The main focus of this Ph.D. dissertation is to tackle these issues and provide scalable and efficient localization solutions while maintaining the accuracy required by many indoor localization applications.

Chapter 2

Basics of UWB-based Localization Systems

2.1 Ultra-widedband Radios

The range of frequencies a radio transceiver uses for TX and RX determines the frequency bandwidth. UWB radios use a wide frequency bandwidth (> 500 MHz) compared to other radios like WiFi that uses 20 MHz or 40 MHz bandwidths. UWB radios use a sequence of pulses that are very short in time (< 2 ns), which requires using an ultra-wide bandwidth. The use of short pulses makes UWB radios resilient to multipath fading, which helps us distinguish the first path of the signal from the multipath components.

For our research, we use Decawave DW1000 [10], a low-power low-cost commercial UWB chip, compliant with IEEE 802.15.4 UWB standard. DW1000 facilitates a reliable and long-range (up to 290 m) communication, which also makes it useful as a connectivity component for IoT applications. DW1000 operates in 3.5 GHz to 6.5 GHz center frequency with bandwidth choices of 500 MHz and 900 MHz. The radio chip can estimate and report the CIR of the received packets along with RX quality information.

2.2 Channel Impulse Response

We can simplify the definition of CIR of a received packet as the energy level received over time. CIR is effective in representing multipath propagation of the received signal. Figure 2.1 shows a typical CIR estimate with LoS and MPCs visible. UWB radios estimate CIR by accumulating the preamble sequence on the receiver side. The receiver correlates the received signals against a known sequence and accumulates correlation values for multiple repetitions of preamble sequence. Then by analyzing CIR, we can find the first path, or LoS, for the signal. Finding the first path helps with finding the precise ToA of the packet. DW1000 uses a threshold-based algorithm to find the first path.

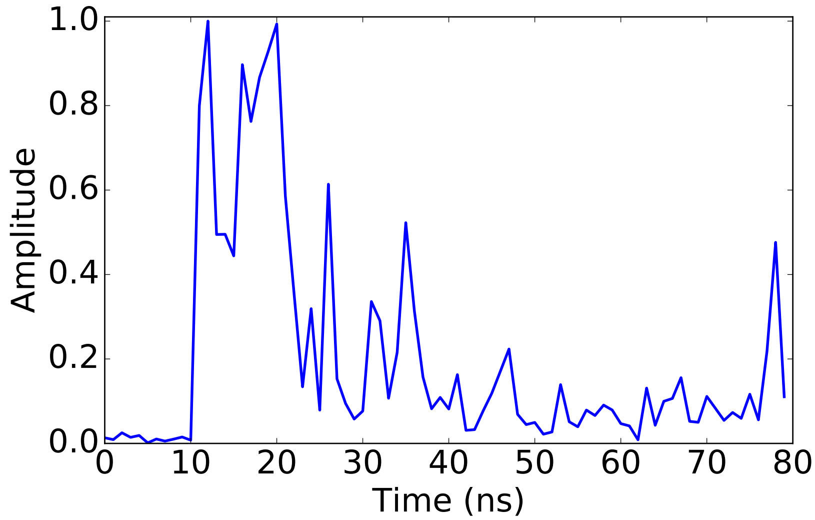

Figure 2.1: Typical CIR at the receiver node with the UWB transmitter at 6 m in complete LoS. The first path arrived at around 10 ns, which is the largest peak. Other peaks belong to MPCs.

2.3 Propagation of Radio-Frequency Signals

Propagation of radio waves in various mediums has different behaviors. NLoS transmission is the transmission of radio signals where a material obstructs LoS between the transmitter and the receiver. As shown in Figure 2.2, when a radio wave hits an obstacle, it may be impacted by one of the following ways:

Attenuation: Amplitude or signal strength may decrease due to the absorption of the signal.

Refraction: Waves may change direction when it goes from a medium to another medium with different density due to change in the propagation speed.

Reflection: Waves may bounce from a smooth object larger than its wavelength.

Diffraction: Waves may bend and change direction around an object, especially the sharp edges, by maintaining their original speed and become a secondary source of waves.

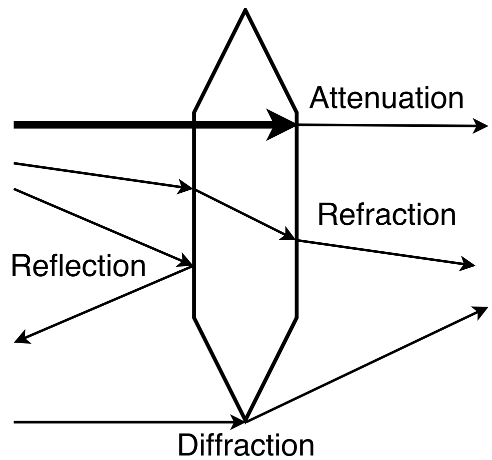

Figure 2.2: Propagation of radio waves when interacting with an obstacle of a different medium. Signals can be attenuated, refracted, reflected, or diffracted.

Signals arriving at an RF receiver always are a combination of the above four phenomena, which makes it challenging to study each of them separately. To reduce or minimize the effect of each of these phenomena, we can design special experimental settings by using absorbent materials or highly reflective materials. An anechoic chamber is a room designed to isolate transceivers from outside noise. The room is covered with highly absorbent materials to absorb signals and prevent reflections. Conducting the experiments in an anechoic chamber minimizes signal reflections and diffractions.

2.4 Ranging

There are several ways to estimate the distance (ranging) between two UWB radio transceivers [43,46]. Many techniques rely on the estimation of time of flight (ToF), the time it takes for a packet to travel from TX to RX. We can then calculate the corresponding distance using Equation 2.1, with v being the propagation speed of electromagnetic waves in the medium. In wireless transmission, v is approximately the speed of light ($\approx 3 \times 10^8$ m/s).

$$d = v \times ToF \tag{2.1}$$

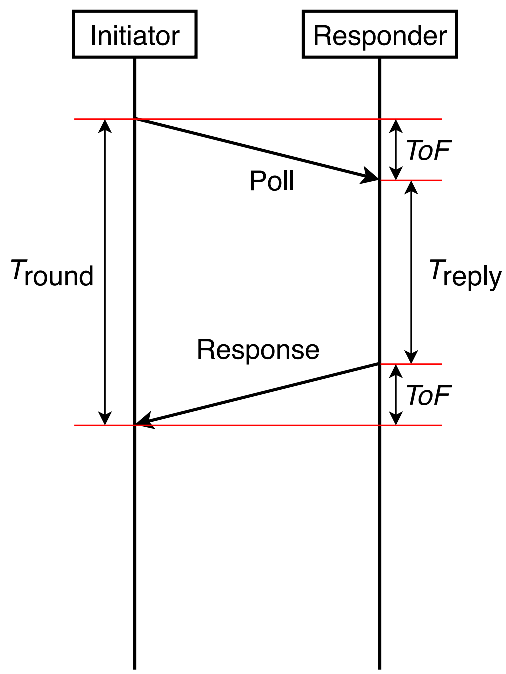

Figure 2.3: Illustration of single-sided two-way ranging. The initiator node sends a ranging poll message. Responder node replies with a message including dynamically calculated T_{reply}, so that the initiator can calculate ToF.

2.4.1 Single-sided Two-way Ranging

Single-sided two-way ranging (SS-TWR) [55], a part of the IEEE 802.15.4 UWB standard [30], estimates the distance between two radio transceivers without needing to synchronize the two devices. As shown in Figure 2.3, the side which estimates the distance (initiator node) sends a ranging poll message. The receiver side (responder node) then replies with a response message, including the dynamically calculated T_{reply} value embedded in the packet. Finally, the initiator uses Equation 2.2 to calculate the ToF.

$$ToF = \frac{T_{\text{round}} - T_{\text{reply}}}{2} \tag{2.2}$$

2.4.2 Asymmetric Double-sided Two-way Ranging

We can use an asymmetrical double-sided two-way ranging method, which is one of the most common and practical UWB ranging techniques in indoor localization, to estimate the range between transceivers. Since DW1000 is capable of reporting ToA of packets with the sub-nanosecond resolution, it enables us to calculate the ToF with decimeter-level precision. Figure 2.4 shows the message exchange protocol. Using the reported timestamps, we can calculate ToF with Equation 2.3 [11].

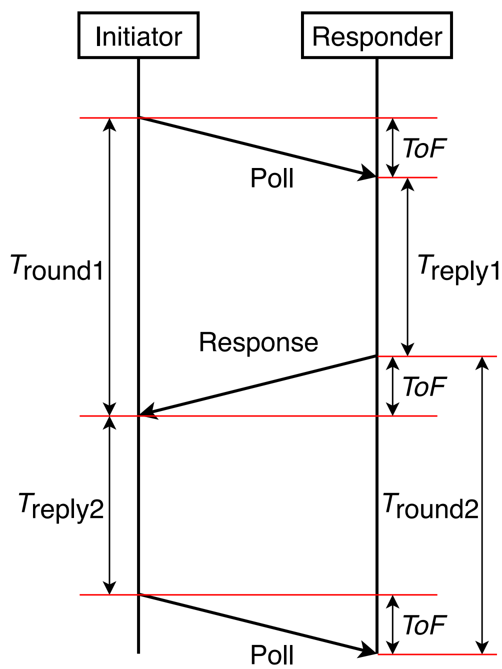

Figure 2.4: Illustration of asymmetric double-sided two-way ranging. First, the initiator sends a ranging poll message. Then the responder sends a response. Finally, the initiator sends a final message, including T_{round1} and T_{reply2}, so that the responder can calculate ToF.

$$ToF = \frac{T_{\text{round1}} \times T_{\text{round2}} - T_{\text{reply1}} \times T_{\text{reply2}}}{T_{\text{round1}} + T_{\text{round2}} + T_{\text{reply1}} + T_{\text{reply2}}} \tag{2.3}$$

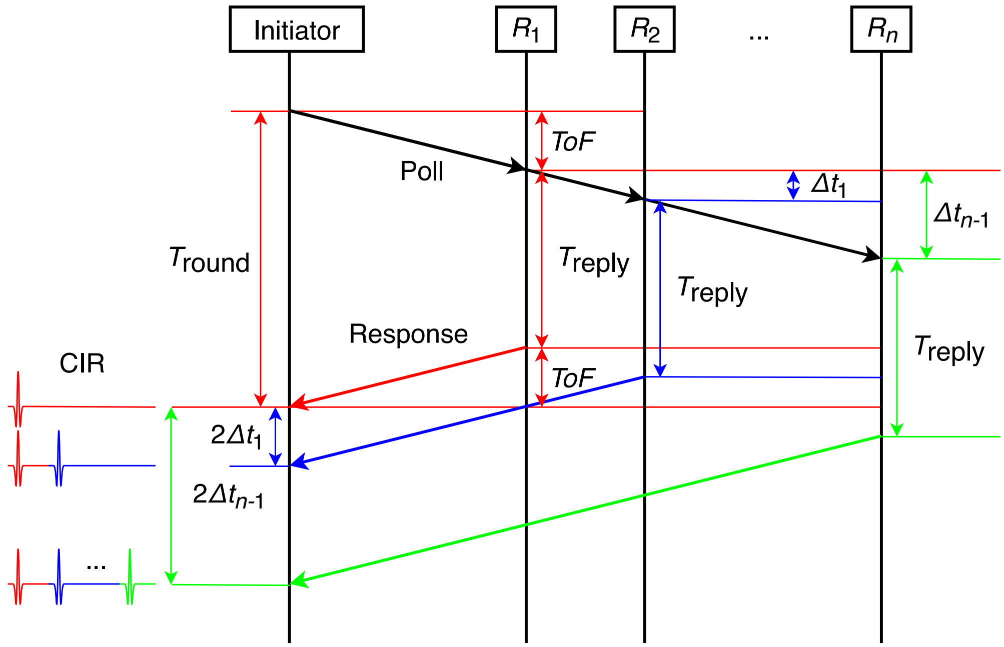

Figure 2.5: Illustration of concurrent ranging. The initiator node sends a ranging poll message. All responders (R_1, R_2, ..., R_n) reply with the same T_{reply} delay. Since R_{i+1} receives the poll message with Δt_i delay, the response from R_{i+1} would be received by the initiator node by $2 \times \Delta t_i$ delay. Although the initiator only receives the packet from R_1, signals from all other responders are visible in the estimated CIR.

2.4.3 Concurrent Ranging

Concurrent ranging refers to a methodology that an initiator radio node measures the distance from multiple responder radio nodes (quasi-)simultaneously. A recent work studied the feasibility of UWB concurrent ranging [6]. As shown in Figure 2.5, the initiator node broadcasts a ranging poll message. Every responder node replies with the same T_{reply} delay. The initiator node receives the response from the closest responder node (R_1) first. All other responses (R_2, R_3, ..., R_n) reach the initiator node with an additional $2 \times \Delta t_i$ delay, with Δt_i being the time difference between the reception of the ranging poll message in R_1 and R_{i+1}. More precisely, the initiator node only receives the packet from R_1, but signals from other responders are also visible in the estimated

CIR. The initiator first calculates its distance with R_1 using Equation 2.2. The initiator node can then calculate the difference in ToF between R_1 and all other responders by analyzing the CIR.

2.5 Angle of Arrival

AoA or angle of incidence is the angle at which a packet arrives at the receiver. A common technique for AoA estimation is to use multiple antennas. When a transmitter is at an angle non-perpendicular to the surface of the receiver antennas, packets arrive at different times at different antennas. We can measure this difference using either the time difference or arrival (TDoA) or the PDoA. Ideally, the receiver radio should be able to switch between different antennas to measure the TDoA or the PDoA. Instead, Decawave proposed to use two receivers running on the same crystal oscillator (XTAL) [15,45]. Figure 2.6 illustrates the idea of AoA estimation with two radios clocked from the same XTAL, along with the Decawave PDoA Node DWM1002, a recently introduced AoA estimation platform with two DW1000 radios. Using the same XTAL is crucial since we need the same time and phase reference for both receivers to be able to measure TDoA or PDoA precisely. Since the timing resolution of DW1000 is not suitable for AoA estimation using TDoA between the two antennas, Decawave suggested using PDoA to estimate AoA [15].

From Figure 2.6, the difference in path length (p) is related to the distance between antennas (d) and AoA (θ) as Equation 2.4.

$$p = dsin(\theta) \tag{2.4}$$

For a carrier frequency, f, the signal wavelength is $\lambda = 2\pi c/f$, where c is the speed of light. PDoA (α) is related to p and λ (or f) as Equation 2.5.

$$\alpha = \frac{2\pi}{\lambda}p = \frac{f}{c}p \tag{2.5}$$

Finally, we can calculate θ as Equation 2.6.

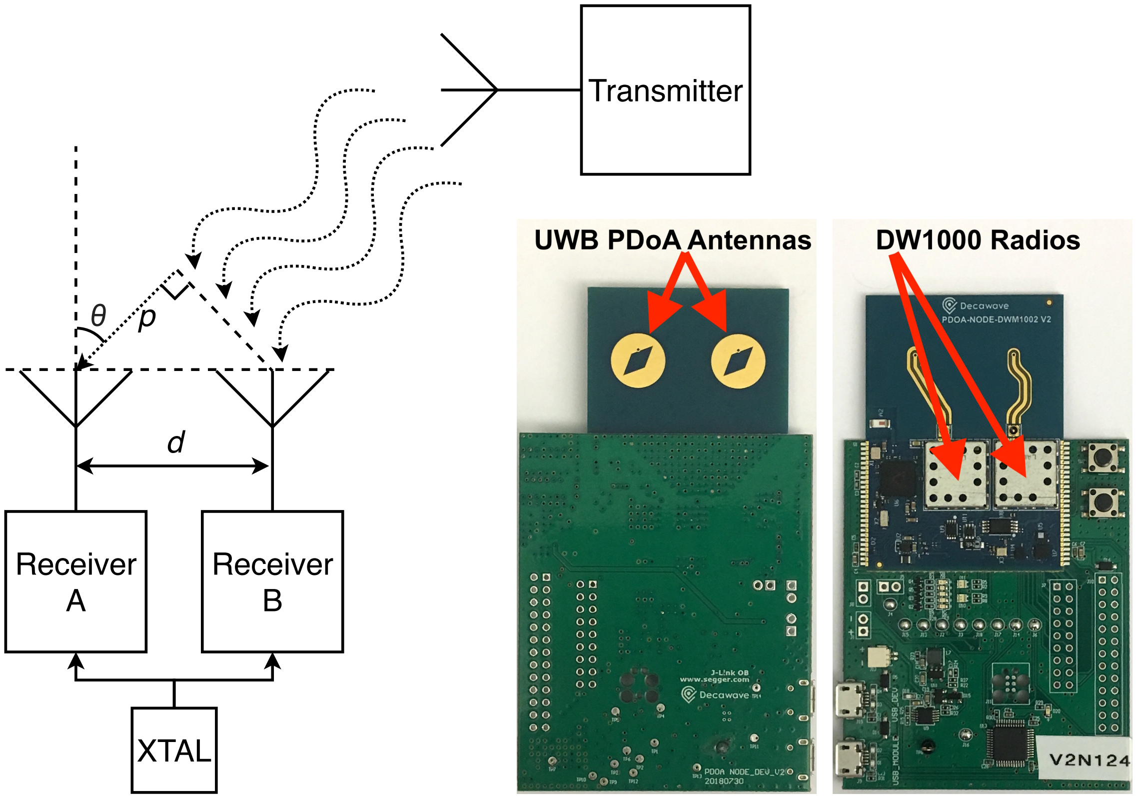

Figure 2.6: Illustration of AoA, and the front and back view of the PDoA node (DWM1002). Two receivers are clocked from the same XTAL to ensure a synchronized frequency. Arriving signals at an angle of θ cause path difference of length p, which makes different PoAs at each antenna.

$$\theta = arcsin\frac{\alpha\lambda}{2\pi d} \tag{2.6}$$

Further, since $-\pi \leq \alpha \leq \pi$, to have a one-to-one mapping between θ and α for $-\pi/2 \leq \theta \leq \pi/2$, we need to place the antennas in a distance such that $d \leq \lambda/2$.

In DW1000, we can use I and Q samples for the first path in CIR for the received packet to calculate the PoA.

2.6 Impact of Timing Limitations on Concurrent Ranging

2.6.1 Transmission Scheduling Uncertainty

The DW1000 chip has a limited TX timestamp resolution. The chip reports the RX timestamp for each packet with a resolution of ≈ 15.6 ps. However, the chip can only schedule the TX time of a packet with a resolution of ≈ 8 ns. Since we schedule the response packets for concurrent ranging by adding a delay to the RX timestamp of the ranging poll message, the TX timestamp has $\pm$ 8 ns of jitter. Consequently, the concurrent signals received by the initiator have the same level of jitter, which causes uncertainty in ToA estimation.

2.6.2 Clock Drift

Oscillators have different behavior over time due to mechanical characteristics and environmental effects such as the change in temperature, vibration, pressure, and voltage. A clock consists of an oscillator to measure time. Embedded devices are usually equipped with a clock to facilitate timing. Any two independent clocks cause inaccuracies that directly affect the performance of UWB concurrent ranging systems. Each concurrent responder should reply with a fixed delay after reception of the ranging poll message, but they cannot count time at the same rate due to clock drift. We can potentially correct these inaccuracies by modeling the clock behaviors.

2.6.2.1 Clock Modeling

With a continuous clock model, $C(t)$ is the time reported by a clock at ideal time t. Clock offset, $\theta(t)$, is the difference between the ideal time and clock time, as shown in Equation 2.7.

$$\theta(t) = C(t) - t \tag{2.7}$$

We can also define relative clock offset for clocks A and B with Equation 2.8.

$$\theta_B^A(t) = C_A(t) - C_B(t) = \theta_A(t) - \theta_B(t) \tag{2.8}$$

Clock skew, $\alpha(t)$, is defined as the first derivative of clock offset. As shown in Equation 2.9, we can estimate the clock skew using the normalized difference of two different offset values in a time period of τ.

$$\alpha(t) = \frac{d\theta(t)}{dt} \approx \frac{\theta(t+\tau) - \theta(t)}{\tau} \tag{2.9}$$

With a discrete clock model, we can estimate the clock skew by re-writing the Equation 2.9 as the normalized difference of offsets in two sequential time steps, $\theta[n-1]$ and $\theta[n]$, as Equation 2.10. Each time step might have a different length. $\tau[n]$ refers to the length of the time period in step n.

$$\hat{\alpha}[n] = \frac{\theta[n] - \theta[n-1]}{\tau[n]} \tag{2.10}$$

Finally, we can define the estimated relative clock skew for clocks A and B as Equation 2.11.

$$\hat{\alpha}_B^A[n] = \hat{\alpha}_A[n] - \hat{\alpha}_B[n] = \frac{\theta_B^A[n] - \theta_B^A[n-1]}{\tau[n]} \tag{2.11}$$

Chapter 3

Related Work

3.1 NLoS RF Propagation Studies

Researchers have characterized the propagation of radio frequency signals through different materials. There is prior work analyzing the impact of building walls and objects on the propagation model and degradation in the reliability of RF communication. Table 3.1 shows that different studies used different settings and materials for NLoS benchmarking. Thus, there is a lack of a standard benchmark in RF propagation studies.

Table 3.1: NLoS RF Propagation Studies

Ref	Frequency Band	Environment	Type of Material
[62]	0.5 to 2 GHz and 3 to 8 GHz	Laboratory	Brick, Brick-faced Concrete, Brick-faced Masonry, Drywall, Uncoated Glass, and Dry Lumber
[63]	0.2 to 3 GHz	Academic Building	Cinder Blocks
[4]	0.9 GHz	Laboratory	Brick and Concrete
[21]	0.5 to 2 GHz and 3 to 8 GHz	Laboratory	Concrete
[61]	0.8 to 6 GHz	Laboratory	Windows with Transparent Conductors
[47]	0.7 to 5 GHz	Residential Building	Not Reported

3.2 Wireless Interference

There is a large body of work that tries to address wireless interference as an issue to avoid, prevent, or mitigate. There is some recent work that tries to leverage interference to improve some aspects of communication.

Interference Avoidance/Prevention: The devices can use random access/back-off style or TDMA style protocols to try to avoid or prevent interference. Another work shows that piggybacking UWB packets over existing network traffic reduces the traffic and avoids collisions [50]. Since carrier sensing is generally not feasible for UWB networks, IEEE 802.15.4 UWB standard suggests ALOHA for channel access [30]. Solutions similar to ALOHA are suitable for scenarios with a small number of wireless nodes, and they cannot scale because the performance drops drastically with an increase in channel utilization beyond 18% [11, 38].

Interference Mitigation: Research has shown the effectiveness of the use of non-linear filters in removing the interference [54]. Another study uses matched filters to mitigate UWB interference and correct for ranging errors [48]. Forward error correction (FEC) or retransmissions are effective methods in mitigating packet corruption or loss in UWB. DW1000-based solutions utilize these standard techniques to make the network work to some extent despite interference. These techniques incur large overhead and work poorly in dense or busy networks.

Interference Exploitation: Concurrent TX from multiple wireless devices is the key component of these solutions. Glossy [18] used concurrent transmissions to build a time synchronization system through network flooding while maintaining the reliability of packet reception. SurePoint [32] exploits concurrent transmissions for flooding-based time synchronization in UWB networks to increase the reliability of packet reception. A relatively new study investigated the feasibility of utilizing concurrent transmissions for UWB-based localization systems [6]. Other studies addressed several technical challenges to improve the performance of concurrency-based localization systems [7, 22, 23]. Another study demonstrated the feasibility and performance of concurrent communication with UWB radios [65].

3.3 Indoor Localization

Table 3.2: UWB-based Indoor Localization Techniques

	Localization Technique	Advantages	Disadvantages
Sequential	Two-way Ranging (TWR)	Accurate Time synchronization is not required	Not scalable High power consumption High air-utilization
	Time Difference of Arrival (TDoA)	Scalable Low power consumption for tags	Accurate time synchronization is required
	Angle of Arrival (AoA)	Low power consumption Low air-utilization Time synchronization is not required	Requires 2 UWB radios per anchor Front-back ambiguity Unknown tag tilting
Concurrent	Concurrent TWR	Saves air-time by using concurrency	Not accurate due to TX timestamping issue Not scalable
	Concurrent TDoA	Saves air-time by using concurrency	Not accurate due to TX timestamping issue Requires antenna delay calibration
	Concurrent AoA **(AnguLoc)**	Saves air-time by using concurrency Low power consumption and air-utilization Accuracy does not rely on TX timestamping	Requires 2 UWB radios per anchor

There are many indoor localization techniques developed, specifically for UWB radios (Table 3.2). Concurrency can increase the efficiency and scalability of indoor localization, but existing concurrency-based solutions fail to achieve the same level of accuracy as sequential measurement solutions.

3.3.1 Concurrent Ranging

Concurrent ranging refers to a methodology in which an initiator radio node measures the distance from multiple responder radio nodes (quasi-)simultaneously. Researchers have studied the feasibility of UWB concurrent ranging [6]. There are several critical issues that we need to address, to be able to build a real-world UWB concurrent ranging. Several research studies identified some of these issues and provided potential solutions [6, 7, 22, 23].

3.3.1.1 Detection of Concurrent Responses in Run-time

A practical UWB concurrent ranging system needs to automatically detect concurrent signal peaks in run-time. Researchers have developed several peak detection and first path detection methods, which the existing research work and patents widely use [6, 17, 29, 33, 44]. However, it is still hard to detect concurrent responses when response signals overlap with each other or when responders are in approximately the same distance from the initiator (equidistant responders), or their MPCs. Using a priori knowledge of the location of the responder nodes helps to detect concurrent signals, but it does not solve the problem of equidistant responders [6] The related work proposed two solutions for automatic peak detection, but they did not comprehensively evaluate such methods for real-world UWB concurrent ranging systems [6, 22]. The first solution is to use a matched filter and correlate the CIR with a pulse shape template to find responder signals. To create different signal shapes, they suggested using different Pulse Generator Delay (PG_DELAY) values. Their method also aims to solve the problem of equidistant responders. However, the overlapping strong MPCs can completely obscure the concurrent signals, which makes it very hard to detect them. The second solution is to mitigate the impact of strong MPCs by using a response position modulation, which adds a delay to each concurrent response to separate them in time. However, we can only fit a limited number of concurrent responses in CIR samples due to its limited size. Combining these two methods can theoretically increase the maximum number of concurrent responses, but it is not thoroughly evaluated in the presence of strong MPCs.

3.3.1.2 Identification of Concurrent Responders

UWB concurrent ranging relies on receiving all the responses within a short time. However, the initiator node only receives one packet (usually from the nearest responder). The initiator then detects concurrent responses by analyzing the estimated CIR for the received packet. Thus, the initiator cannot use any high-level (e.g., packet-level) identification information inside the concurrent responses. Using different pulse shapes (by using different PG_DELAY) for each responder and using a matched filter can potentially help identify the individual senders [22].

3.3.1.3 Ranging Error Due to Clock Drift

Typically, responders use independent frequency oscillators, which can drift against each other due to both environmental effects and mechanical differences. Since we measure the difference in the distance only using the difference in the ToA, each responder needs to minimize the jitter in its reply time. Hence, every responder adds a constant delay to the RX time of a request packet to calculate the TX time of the response packet. Since this time delay is referenced to a local frequency oscillator, the actual TX delay is not consistent with other responders. The jitter in the TX time caused by clock drift causes inaccuracy in ToA of concurrent signals received by the initiator node. One technique to address this problem is to minimize the constant delay so that all responders transmit as fast as possible to reduce the clock drift-induced error [6]. Minimizing the delay requires a specific set of radio configurations and specialized software on the main processor. For the DW1000 chip, each preamble symbol duration is ≈ 1 µs [11]. The chip supports preamble lengths up to 4096 symbols. Since the radio needs to send the preamble before the scheduled TX time, the 330 µs delay used in the recent studies requires using a maximum preamble length of 256 symbols [6]. However, achieving longer ranges requires longer preamble lengths [11]. Also, the specialized software should be fast enough in reading and processing the packet to be able to minimize the delay, which limits its functionalities. To solve this problem, we use a clock skew correction method based on time transfer techniques. Researchers have developed several time transfer methods [18,42,68] to synchronize independent clocks, and frequency oscillator disciplining methods [14, 40] to synchronize the frequency of local oscillators. Our work uses a clock skew estimation technique similar to [35, 53].

3.3.2 Concurrent Time Difference of Arrival

Existing concurrency-based localization systems (e.g., SnapLoc [23] and Chorus [7]) use ToA information for all concurrently received packets. The main problem with *concurrent* localization systems is their failure to achieve high resolution timestamping that *sequential* localization systems can achieve, which affects the quality of location estimates, i.e., 1.0016 ns for concurrent vs. 15.6 ps for sequential on DW1000 platform. On the contrary, AoA estimation only relies on phase information and is not affected by timestamping jitter.

3.3.3 Angle of Arrival

Many research studies explored various ways to measure AoA [31, 66, 67], including by calculating the PDoA using two radios clocked from the same crystal oscillator [15,45]. AoA-based localization systems typically face front-back ambiguity and AoA receiver unknown tilting problems. One way to address these two challenges is to measure AoA on the anchors' side and assume known tilting [64, 67]. Researchers developed methods to address the unknown tilting problem, but they assumed no front-back ambiguity on the angle measurements [58, 71]. Another research study uses at least 3 UWB radios on a circular shape, clocked from the same frequency oscillator, for the anchor to concurrently estimate the location of 3 tags by combining the ToF and phase information. However, their proposed method cannot scale the number of tags [66].

Chapter 4

Toward Standard Non-Line of Sight Benchmarking of UWB Radio-based Localization

UWB radios have received significant attention in the past few years after the development of affordable commercial chips like DW1000 [9] by Decawave [1]. UWB radios facilitated precise indoor localization due to the capability of estimating the ToA of wireless packets in sub-nanosecond level; hence it drew the attention of researchers and even made its way to industrial solutions. While researchers proved that UWB-based localization techniques are viable solutions, yet there is no benchmarking standard to fully understand the localization performance in different scenarios. It is difficult to make a systematic comparison between proposed solutions without a proper performance evaluation standard; furthermore, the evaluation scenarios typically used in research are not similar to real-world deployment environments.

Researchers developing new UWB-based, including Decawave-based, localization systems, evaluate their new approaches typically in LoS scenarios, and occasionally also in NLoS scenarios. The reason to include these scenarios in their evaluation is that they want to mimic realistic environments, which consists of a mix of LoS and NLoS scenarios. LoS scenarios are well-defined and generally mean no visual obstruction between the tags and the anchors used in UWB localization experiments. Unfortunately, we have found no consistent definition of NLoS scenarios. It appears that the researchers are using walls or other types of obstruction as NLoS, i.e., visual NLoS scenario. While the intention of the researchers in incorporating NLoS experiments is commendable and is in the right direction for the field, without understanding UWB propagation properties of UWB through those obstructions, it is difficult to not only compare results from different publications but also to know if we are truly evaluating UWB-based localization where the tags and the anchors may have "difficult" obstructions in-between: a thin paper may create a visually NLoS scenario. However, it will not have much impact on localization performance. Thus, NLoS is loosely defined; hence it is interpreted differently in various contexts.

From a technical standpoint, there is a clear difference between LoS and NLoS scenarios. A radio signal, when LoS is obstructed, can be attenuated, refracted, reflected, or diffracted. The receiver always receives a combination of the signals mentioned above with different proportions. Although visual NLoS blocks LoS between transceivers, a large proportion of radio signals may still be able to penetrate the obstructing material. Refracted signals are delayed compared to the LoS signal; hence they add a positive bias to ToA observed by the receiver, which translates to ranging bias in distance estimation and localization applications. With prior knowledge of the environment, including possible sources of reflection, and obstructions' shape and material, we may be able to correct the positive bias caused by the delayed signals. The localization techniques developed by researchers routinely use these properties of UWB propagation through obstacles. If NLoS is interpreted inconsistently, a technique that claims to work well in one NLoS scenario may not work well in an NLoS scenario replicated by another researcher. In fact, this has been one of the challenges in the field of UWB-localization because researchers have found it challenging to replicate the results reported by others despite a large number of researchers using the same Decawave chips.

It can be extremely challenging to identify what truly happens to radio signals, especially in real-world dynamic NLoS scenarios. With the lack of a proper benchmarking standard, research studies created their own test scenarios to evaluate their proposed localization solutions. Since it is hardly possible to create exactly the same customized test environments from one study in another one, it is impossible to correctly compare their results. Furthermore, the physical properties of the obstructing material, even if the same material is used, affect the behavior of radio signals: (1) Thickness and substance affect attenuation and refraction. (2) The smoothness of the surface affects reflection. (3) Shape and thickness of edges affect diffraction. The two latter cases are harder to characterize when we try to understand NLoS scenarios in a typical test environment.

We take the first steps toward standard NLoS benchmarking to understand how attenuation and refraction affect radio signals. Our contributions are:

- We present a methodology to observe the effects of attenuation and refraction on UWB radio signals by minimizing reflection and diffraction.
- We explore the true effect of attenuation and refraction on UWB radio signals when the signal propagates in different construction materials.
- We present scenarios where NLoS ranging performance of UWB radios are severely affected by NLoS. However, it is impossible to identify and mitigate without the use of fingerprinting and a proper amount of learning data.

4.1 How Do We Evaluate NLoS UWB Today?

Features like large bandwidth, low duty cycle, and high penetration rates enabled UWB indoor localization systems to achieve accuracies around 10 cm [2]. Three most popular techniques used in UWB indoor localization are ToA estimation and ranging [28], TDoA [36] and AoA estimation [70] (e.g., using PDoA [15, 25]). All these techniques use LoS signals to estimate the location of the target. In all the mentioned approaches handling NLoS signals is a real challenge. We can categorize the literature work in this area into two sections: Avoiding NLoS signals [6, 32] and utilizing NLoS signals [13]. In avoiding NLoS approaches, the focus is on increasing the chance of receiving the

Table 4.1: State-of-the-art UWB Localization NLoS Evaluation – Experimental Setup

Ref	**Test Environment**	**Type of Material**	**Most Probable Material**
[56]	Lab/office	Tables and chairs	Wood
[5]	Road construction site	Vehicles, Loader	Metal
[51]	Lab/office, coffee shop, and dining hall	Furniture	Wood
[49]	Academic building and coffee shop	Walls and furniture	Concrete and wood
[69]	Corridors and classrooms	Walls, doors, and desks	Concrete and wood
[24]	Corridor, indoor offices, and parking areas	Not reported	Concrete and wood
[60]	Residential apartment	Not reported	Wood and brick
[13]	Room in a commercial building	Not reported	Wood
[59]	Heavy machines lab	Metallic surface and motors	Metal
[32]	20 m $\times$ 20 m area in an academic building	Not reported	Concrete and wood
[20]	Office space	Not reported	Wood
[16]	Hole in a building	Not reported	Concrete
[34]	A lecture room, a cluttered laboratory, and a corridor	Not reported	Concrete and wood
[41]	Several offices, hallways, one laboratory, and a large lobby	Not reported	Concrete and wood

LoS signal either by using more antennas and links or detecting NLoS signals and discarding them. In utilizing NLoS techniques, NLoS signals are added to LoS to improve the robustness of indoor localization systems. These approaches do not try to distinguish between NLoS and LoS signals. Despite the advancements in both categories (avoiding/utilizing NLoS), the lack of a common standard to evaluate these works is obvious. In Table 4.1, we summarized experimental setups used by literature work in the UWB localization area for performance evaluation of their system. As shown in Table 4.1, there is no common ground to compare the proposed work. Since, in most of the related work, the authors did not precisely specify the type of materials in their test environment, we had to guess the material based on the experiment's environment. It is essential to mention that competitions like Microsoft Indoor Localization provide a common environment to evaluate indoor localization systems. However, they require all the competitors to bring and set up their systems in a specific location. The focus of our work is providing guidelines toward standard benchmarking of indoor localization systems. Researchers at TU Berlin also started some work toward the standardization of indoor localization systems [37]. They proposed a framework to collect location estimations and ground truth information and also calculate statistical information about the accuracy of indoor localization systems under test.

The lack of evaluation standard is more severe in NLoS identification techniques since the main idea in such works is utilizing differences between LoS and NLoS signals. Recently researchers pointed out the visual NLoS challenge in which walls and objects obstruct the LoS signal, but the received signal still is very similar to the LoS signal [24]. This phenomenon severely degrades the performance of previous work in NLoS identification/mitigation area [24]. Decawave (the manufacturer of DW1000 chips) also studied the problem of visual NLoS signals [19,52]. Our results also indicate the similarity of LoS signals with visual NLoS signals. One way to detect NLoS is to compare the signal's power with the first path power [24]. We show that such techniques are not reliable in cases where there are not enough multipath components in the received signals.

4.2 Experiments

We conducted experiments with different construction materials in an anechoic chamber to understand how signal attenuation, refraction, and diffraction affect the performance of UWB ranging. Figure 4.1a and 4.1b show the experimental setup in an anechoic chamber. We divided the chamber into a small room and a large room by placing an aluminum shielded object between the two rooms. We placed the transmitter node inside the small room and the receiver node inside the large room. Despite using an RF-opaque shield, communication is still possible through diffracted signals. We

(a) Complete NLoS created by the aluminum-covered signal shield. No communication is possible.

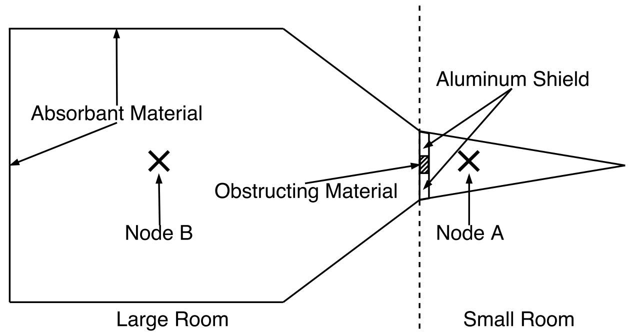

(b) Experimental setup in an anechoic chamber, showing the receiver node and aluminum-covered signal shield, allowing signals to go through only the obstructing material.

Figure 4.1: Anechoic chamber

confirmed that the transceivers could communicate when we removed the diffraction effect by completely covering edges of the signal shield with signal absorbent walls. Although the signal shield is covered by multiple layers of aluminum, we verified that one layer of aluminum with a thickness of 0.024 mm is sufficient to completely block signals and no communication would be possible. Further, we cut a 158 mm $\times$ 158 mm hole in the shield to allow signals to reach the receiver node. Then we covered the hole with different construction materials so that signals can only go through the obstructing material. We chose a set of commonly used construction materials in many buildings so that we can understand how signals propagate in real-world scenarios. Table 4.2 shows a list of the construction materials we used in our experiment, which we purchased from Home Depot. This method enables us to observe the pure effect of signal attenuation and refraction caused by different materials. We used two radinoL4 DW1000 as our transceivers and implemented an application to collect ranging data, implemented as asymmetrical double-sided two-way ranging, along with CIR and RX quality information. Transceivers were placed in approximately 3.86 m apart from each other, operating in UWB channel 2 (4 GHz center frequency and 500 MHz of bandwidth), with preamble length of 2048, and data rate of 110 kbps.

Table 4.2: Construction Materials Used in NLoS Experiments

Material	Paver Brick	Ceramic	Porcelain	Drywall	Rumble Stone	Glass	Wood	Granite	Concrete
Thickness (mm)	59	5	5	10	43	2.4	20	10	58

4.2.1 Single Materials

4.2.1.1 CIR Analysis

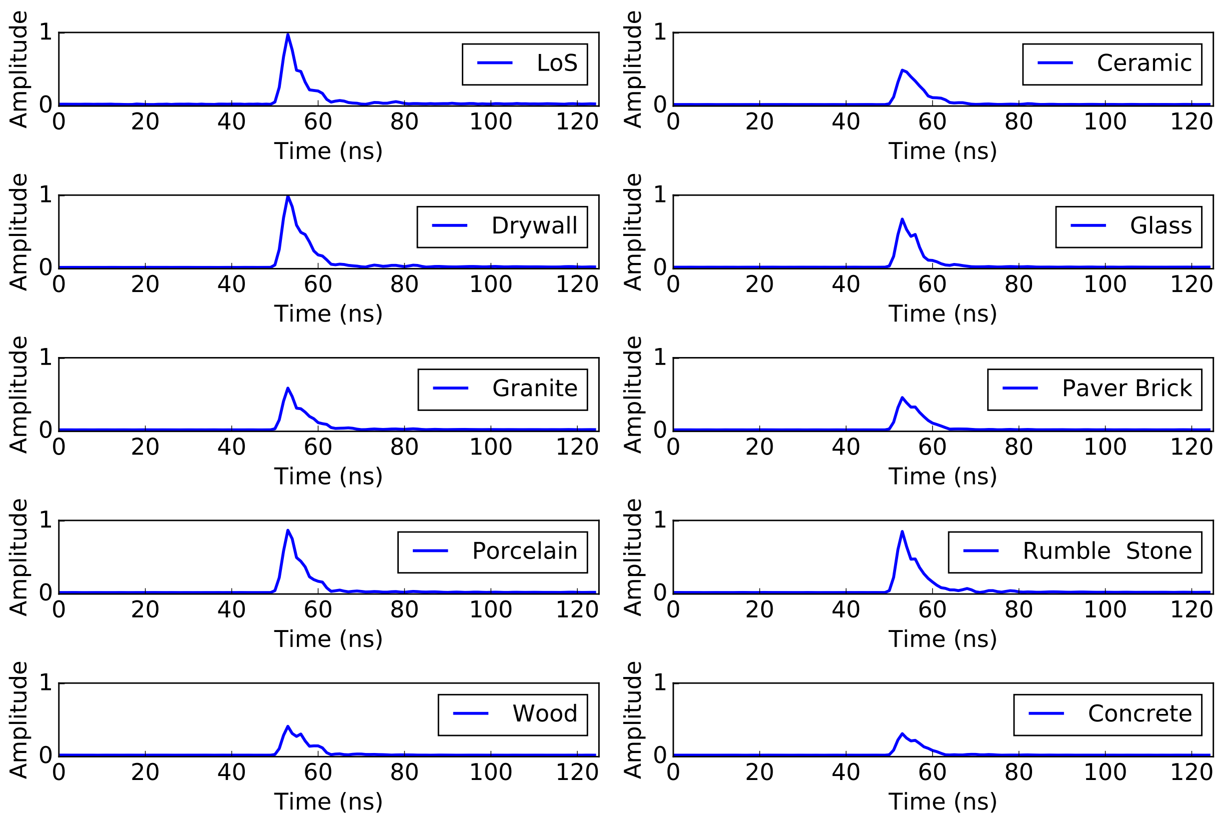

Figure 4.2: CIR impacted by different materials obstructing LoS. Signals get attenuated and amplitude of CIR is decreased.

Due to the ultra-wide bandwidth of UWB signals (500 MHz), high resolution (1 ns) estimate of CIR is possible in UWB communication. CIR represents the UWB channel, as many studies have utilized CIR to find differences in LoS and NLoS signals. In our experiments, only the NLoS signals which traveled through the obstacle arrive at the receiver. We compare the estimated CIR of the received signal to study the impact of different materials on channel characteristics. Figure 4.2

illustrates CIR information after changing the obstructing material between the transmitter and receiver. As shown in Figure 4.2, despite the changes in amplitude values, the overall pattern of CIR remains the same and very similar to the original LoS (not obstructed) signal. Figure 4.2 clearly shows the similarity between LoS and obstructed signals.

4.2.1.2 RX Power Level Analysis

When signals travel through an obstacle, they get attenuated and lose energy. We observe this effect in Figure 4.3, showing the amount of received signal strength as an indicator of the impact of different materials. Concrete has the highest impact on power and drywall has the lowest impact.

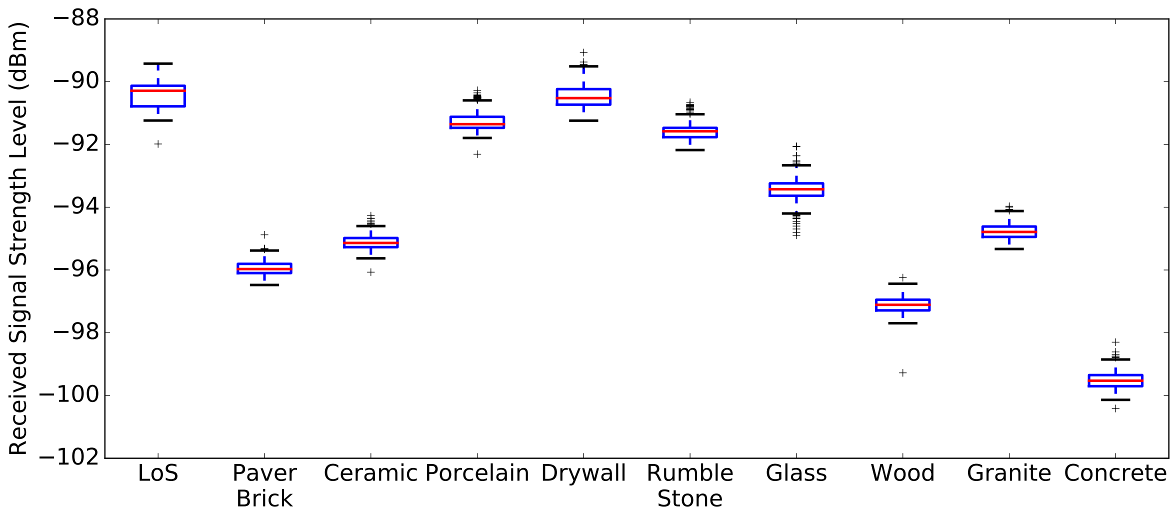

Figure 4.3: RX signal strength impacted by different materials obstructing LoS. Signals get attenuated and the signal power is decreased.

4.2.1.3 Ranging Bias

NLoS propagation of UWB signals through different materials causes the signal to be attenuated and refracted. Refraction changes the propagation speed of signals and adds a delay, which translates to ranging bias. Ideally, attenuation and decrease in received signal strength should not impact ranging accuracy, but previous studies show that ranging has a bias varying with received signal level [3]. Figure 4.4 shows ranging bias caused by different materials, with paver brick having the largest bias.

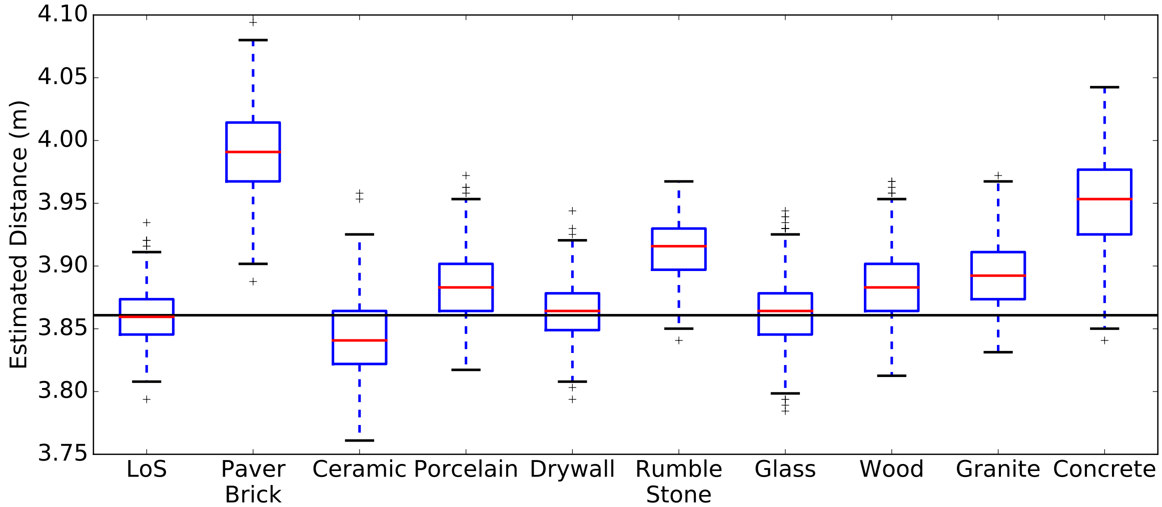

Figure 4.4: Reported range impacted by different materials, obstructing LoS. The horizontal solid line represents the actual distance of 3.86 m. The combined effect of attenuation and refraction of signals adds a ranging bias.

4.2.2 Composite Materials

We conducted a few experiments to analyze the impact of composite materials on UWB signals. In each experiment, two layers of different materials are obstructing the LoS signal.

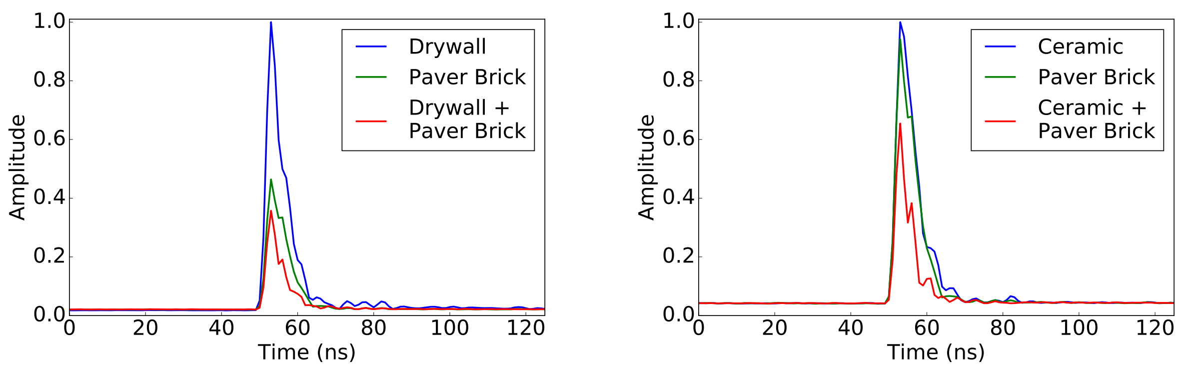

(a) Drywall and Paver

(b) Ceramic and Paver

Figure 4.5: CIR impacted by composite materials obstructing LoS. CIR peak amplitude decreases, but the shape remains the same.

4.2.2.1 CIR Analysis

Figure 4.5 illustrates the estimated CIR values after obstructing LoS with two layers of materials. Figure 4.5a and 4.5b show the impact of single materials on UWB signals separately and once they are put together to obstruct signals. Multiple layers of different materials, decrease the amplitude of signals more, but the shape still is the same as LoS signal.

4.2.2.2 RX Power Level Analysis

Figure 4.6 shows the effect of composites on the RSS level, compared to single materials. The impact is higher compared to single materials.

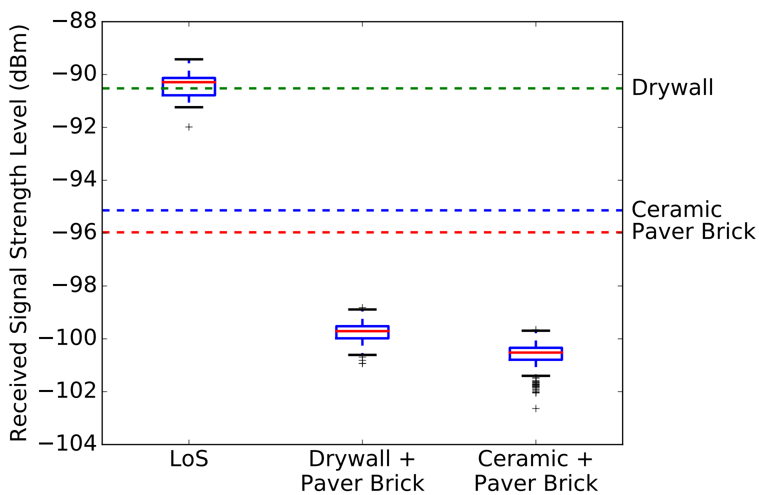

Figure 4.6: RX signal strength impacted by different composite materials obstructing LoS. Horizontal dashed lines are median RSS for single materials. Signals get attenuated more than single materials.

4.2.2.3 Ranging Bias

Figure 4.7 shows the effect of composites on range estimate accuracy. The impact is higher compared to single materials.

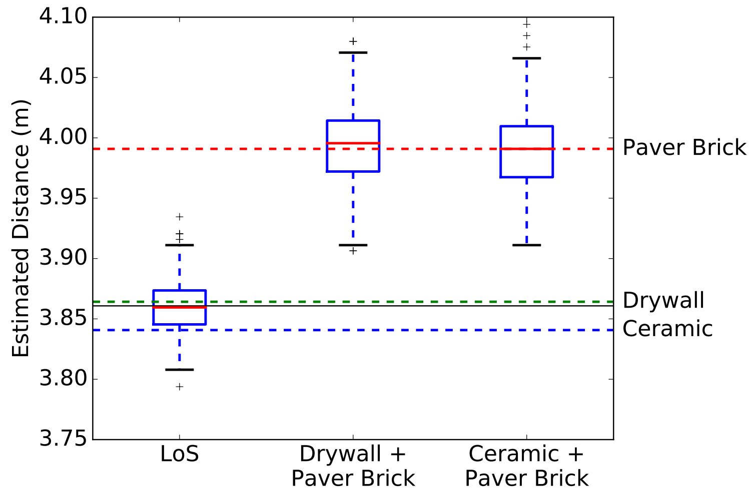

Figure 4.7: Reported range impacted by different composite materials obstructing LoS. The horizontal solid line represents the actual distance of 3.86 m. Horizontal dashed lines are the median distance for single materials. Signals get attenuated and refracted more than single materials, which adds more ranging bias.

4.2.3 Diffraction

In another experiment, we explored the effect of diffracted signals on ranging accuracy. We blocked LoS between transceivers with an aluminum shield, but this time we allowed signals to be diffracted, so the communication is possible. The experiment setup is shown in Figure 4.8. The actual distance between transceivers was 407 cm, but the estimated distance has a median of 405.18 cm. As shown in Figure 4.8, we can calculate the total distance that signals traveled as $d_1 + d_2 = 405.87$ cm.

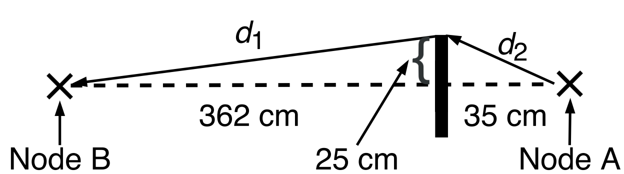

Figure 4.8: Illustration of diffracted signals. Diffracted signals take a longer path than LoS; hence, the estimated distance should be larger than LoS.

4.3 Implications

There are three main implications from the results of this benchmarking work.

4.3.1 Careful Configuration of Anechoic Chamber Experiments

Despite being common knowledge, separate impacting factors of NLoS RF propagation is not investigated in UWB-based indoor localization studies. Observing only the combined impact of attenuation and refraction requires removing reflection and diffraction by shielding the transmitter in an anechoic chamber and allowing signals to only go through obstruction materials. Observing only the impact of diffraction requires using an RF-opaque shield in an anechoic chamber.

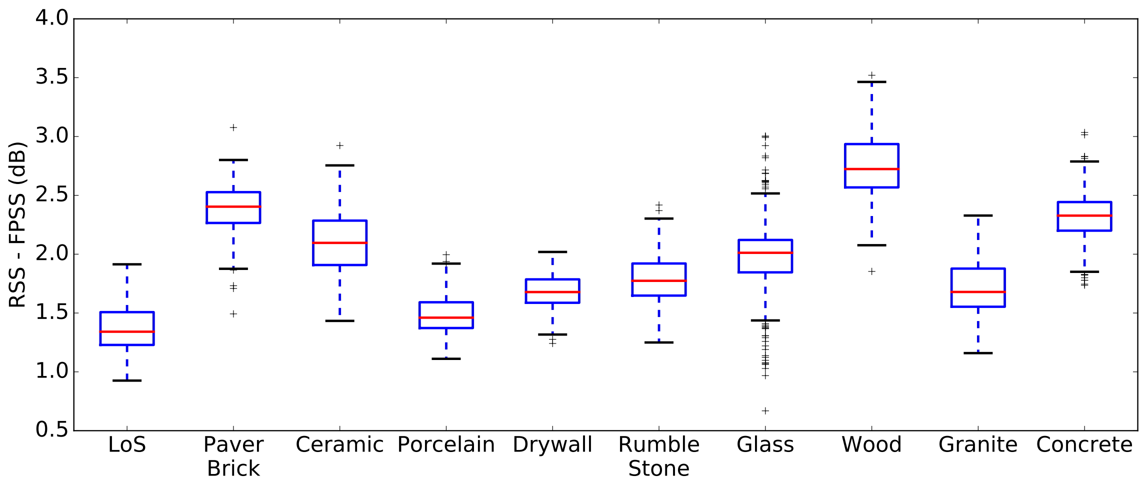

Figure 4.9: The difference between total RX power level and first path power level with a single-layer material obstructing LoS. The difference is less than 2 dB. Small difference makes LoS and NLoS hardly distinguishable.

4.3.2 Limitation of Existing NLoS Identification Approaches

NLoS identification approaches mainly rely on the differences between LoS and NLoS signals to accurately detect NLoS signals. Our results show that in the absence of MPCs, LoS and NLoS signals are very similar to each other, making them hardly distinguishable. Recent work on NLoS identification is to determine if the difference between total RX power and the first path power is larger than 6 dB [24]. Figure 4.9 shows that the difference between the total RX power level and first path power level is less than 2 dB in our experiments with single-layer materials obstructing the LoS. Figure 4.10 shows that such difference is less than 3 dB with composite materials. We can conclude that without enough MPCs, NLoS is not easily distinguishable from LoS.

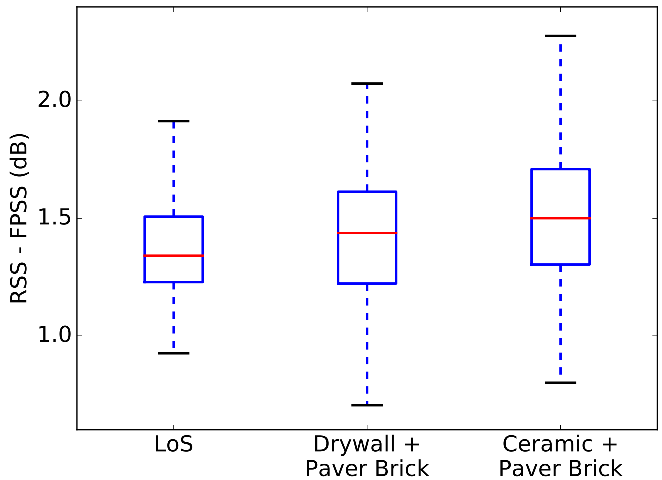

Figure 4.10: The difference between total RX power level and first path power level with composite materials obstructing LoS. The difference is less than 3 dB. Small difference makes LoS and NLoS hardly distinguishable.

4.3.3 Benchmarking

We showed that different materials have different impacts on UWB-based localization performance, which means any benchmarking effort should specifically identify and report types of materials used in the testing environment. Furthermore, by identifying the materials in the test environment, researchers might be able to model the ranging bias more accurately.

4.4 Conclusions

We identified an important problem in the domain of UWB communications and indoor localization applications. The lack of a proper standard in benchmarking and neglecting the difference between visual NLoS and RF NLoS makes the results of different studies non-comparable. We are the first to systematically propose methods for evaluating UWB-based systems in NLoS scenarios. Separately observing each impacting factor in NLoS RF propagation (reflection, attenuation, refraction, and diffraction), helps to understand these impacts better in more complicated scenarios. We verified the reproducibility of results in time, by redoing the measurements after 40 days in the same anechoic chamber.

Chapter 5

R3: Reflection Resilient Concurrent Ranging with UWB Radios

With the daily increase in the number of IoT devices, it is necessary to build a localization solution that is power efficient and can scale to large networks. Furthermore, as location tracking systems are especially useful in mobile applications, it is important to be able to estimate and obtain location information of the devices frequently, often several times per second. Concurrent ranging with UWB radios aims to tackle this challenge by making use of the CIR of concurrent packets and (quasi-)simultaneously measuring the distance from multiple responders based on the difference in their ToA [6]. However, existing solutions for concurrent ranging are not practical in real-world environments due to critical scalability issues.

Concurrent ranging is ideally more efficient than conventional ranging methods. In a typical ranging scenario, an initiator node has to exchange packets with every responder node separately. This method requires either a separate request and response between the initiator node and each responder node or one request from the initiator node and sequential responses from all responder nodes. The latter requires time scheduling for all responder nodes to determine their time of transmission. In concurrent ranging, the initiator node measures the distance from all responder nodes by sending one request. The responders send their responses concurrently. Thus, the response packet received by the initiator node contains signals combined from multiple responders. The initiator then extracts ranging information from the CIR of this concurrent response packet. This way, the number of required packets is drastically reduced, and there is no need for scheduling between the responder nodes. Consequently, concurrent ranging is less power-hungry, has less air utilization, and it is faster.

Concurrent ranging faces several critical challenges in real-world applications such as automatic detection of responses in run-time, detection of responses overlapping with MPCs, and failure to maintain ranging precision and accuracy due to hardware timestamping uncertainty and clock drift. Existing research work proposes solutions for such challenges [6, 22]. To automatically detect concurrent responses in run-time, one study suggests either using a power boundary to filter MPCs, or to exploit a priori knowledge about the environment [6]. Another study suggests either mitigating the overlapping signals from multiple transmitters by having different transmitters use different pulse shapes (PG_DELAY values) and correlating a signal shape template with the estimated CIR of the received packet or avoiding the overlapping by delaying each response to separate them in time [22]. However, these solutions fail in the presence of strong MPCs and are not scalable due to the limitation on how long CIR data can be and also due to clock drift. One method to solve the ranging accuracy issue caused by clock drift is to minimize the response delay for each responder node to minimize the clock drift [6], which prevents long-range communication due to limitation in using proper radio configurations. A potential solution to the ranging precision issue caused by timing limitations is to use multiple rounds of concurrent ranging, but it can limit the location update rate. We need to identify how many rounds of ranging are sufficient to achieve sub-meter ranging precision.

We take steps toward a practical UWB-based concurrent ranging solution and tackle the challenges mentioned above. We present R3, a Reflection Resilient Ranging solution, and specifically target the problem of scalability in concurrent ranging with UWB radios using two techniques. First, we propose a methodology that enables us to detect concurrent responses in run-time, even in the presence of strong MPCs. We are the first to identify how many concurrent ranging rounds are required to achieve sub-meter ranging precision. Second, we relax time constraints on the response delay by using a clock skew correction method to achieve a higher operating range. R3 reduces the ranging error in long distances (> 50 m) by at least 54 cm and by 97% on average for arbitrarily large ranging response delays, compared to when we do not use a clock skew correction method.

In this chapter, we focus on these contributions:

- Design an algorithm to detect concurrent responses in run-time, resilient to strong reflections.
- Relax responder processing time constraints by using a clock skew correction method.
- Implement and evaluate R3 on Decawave TREK1000 [12].

5.1 Empirical Observations

We discuss the empirical observations we made while experimenting with concurrent signals and MPCs on our UWB testbed. These observations inform the design of R3.

5.1.1 Multipath Deviation

The DW1000 chip has a limitation in the resolution of the TX timestamp. The chip reports the RX timestamp for each packet with a resolution of $\approx$ 15.6 ps. However, the chip can only schedule the TX time of a packet with a resolution of $\approx$ 8 ns. Since we schedule the response packets for concurrent ranging by adding a delay to the RX timestamp of the ranging poll message, the TX timestamp has $\pm$ 8 ns of jitter. Consequently, the concurrent signals received by the initiator have the same level of jitter, which causes uncertainty in ToA estimation.

If we repeat concurrent ranging, we can align signals from R_1 so that the jitter only accumulates on the other responders' signals ($R_{i>1}$). As illustrated in Figure 5.1, MPCs for each responder signals have similar time distribution compared to their first path signal. However, signals from R_2 have a larger time deviation compared to signals from R_1 due to the hardware timestamping uncertainty.

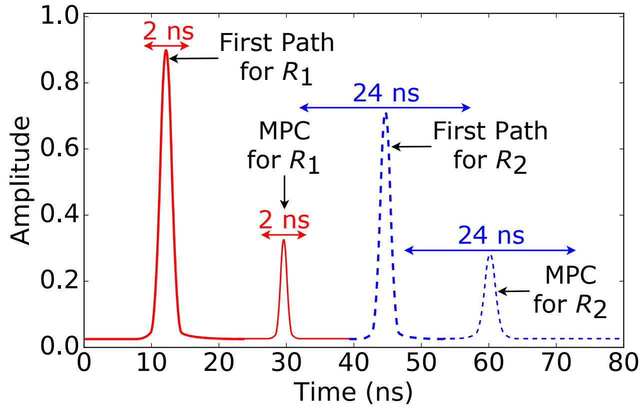

(a) Theoretical illustration of peak time distribution.

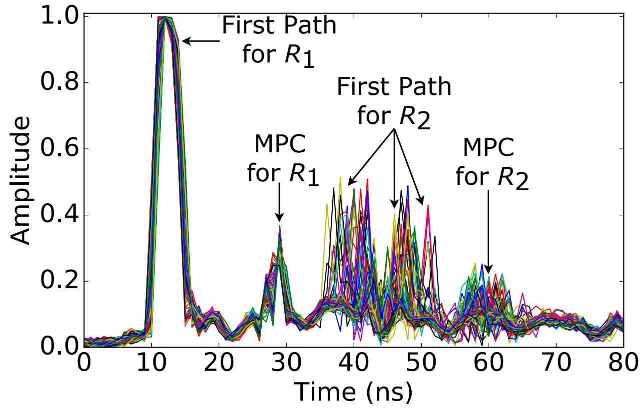

(b) Estimated CIR for 100 packets with packets received from both R_1 and R_2.

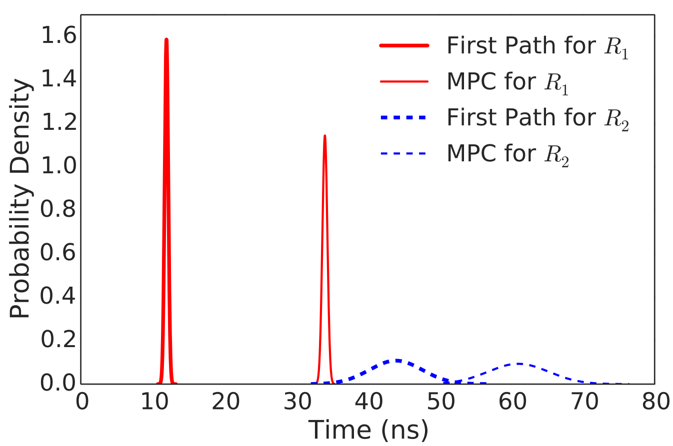

(c) Empirical illustration of peak time distribution.

Figure 5.1: Illustration of peak time distribution for signals from concurrent responders (R_1 and R_2). Signals from R_2 have more time deviation than the MPCs for signals from R_1.

5.1.2 Multipath Amplitudes and Power Boundary

One method to reliably detect concurrent responses is using a power boundary [6]. The rationale behind this is if MPCs have the same power level as the first path, they remain below the power boundary since they traveled a longer path. However, in reality, signals can constructively interfere with each other resulting in strong MPCs with very large amplitudes. Figure 5.2 shows CIR for concurrent responses from R_1 and R_2. Strong MPCs can easily exceed the power boundary and make it challenging to detect concurrent responses. Thus, despite the suggestion in the literature, our solution cannot entirely rely on MPCs not exceeding the power boundary.

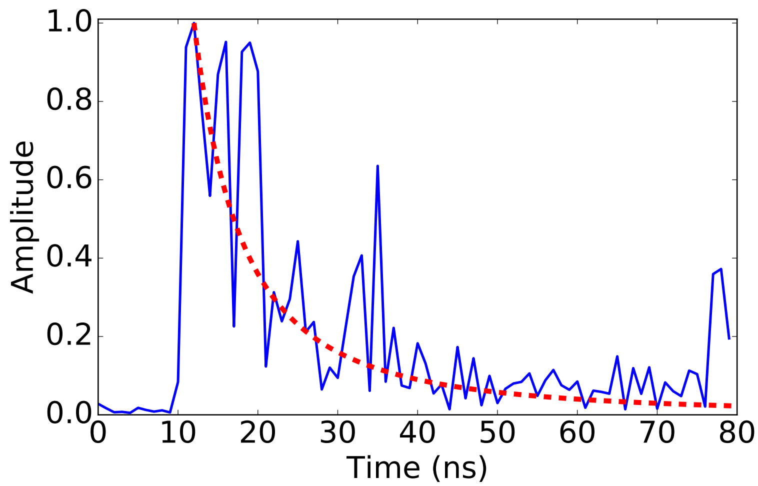

Figure 5.2: CIR for two concurrent responders ($R_1 + R_2$) and a power boundary. MPCs can easily exceed the power boundary and make it challenging to detect concurrent response peaks.

5.1.3 Wired vs. Wireless Experiments

To study UWB concurrent ranging in a controlled environment, we may need to remove MPCs. Conducting experiments in an anechoic chamber, in which the walls are covered with RF-absorbent materials, is helpful to minimize MPCs. However, in some experiments, we need larger distances that require very large anechoic chambers that might not be easily accessible. Another option is to directly connect radio transceivers using RF coaxial cables. Figure 5.3 shows CIR for a typical concurrent ranging scenario with an initiator and two responder nodes. We can easily see that a wired experiment setup removes MPCs and make it easier to see concurrent ranging signals. Figure 5.1b shows CIR for 100 packets collected from R_1 and R_2, where MPC is created by attaching an RF coaxial cable with one end left open. We also need to be aware of the difference in the propagation speed of RF signals on the air ($\approx 3 \times 10^8$ m/s) and in RF coaxial copper cables ($\approx 2 \times 10^8$ m/s), which is very important in calculating the distance between responder nodes based on the difference in ToA of signal peaks.

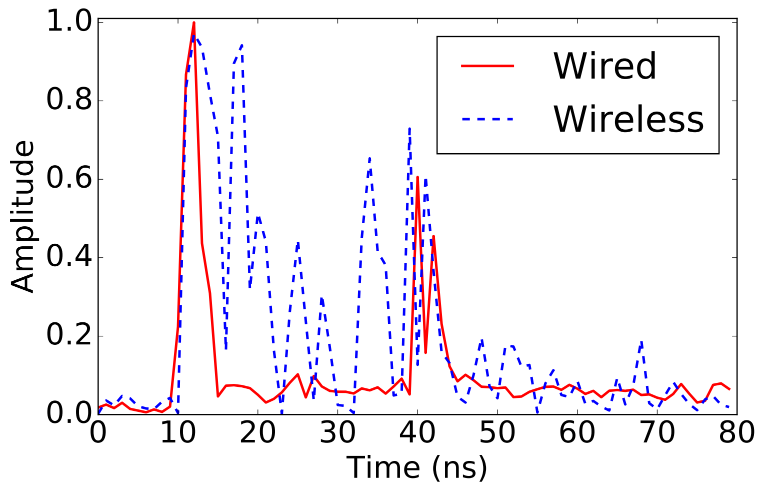

Figure 5.3: Comparison of CIR in wired and wireless setups for concurrent ranging experiments with two responders (R_1 and R_2). We can easily detect the R_2 signal in the CIR for wired setup (around 40 ns). Multipath propagation of wireless signals creates a lot of strong MPCs, making it very hard to detect the R_2 signal.

5.2 System Design

In concurrent ranging systems, an initiator node concurrently measures the distance from multiple responder nodes by measuring the difference in the ToA of their response to a poll message. Typically a radio transceiver can only receive one packet at a time. Therefore, concurrent ranging cannot rely on receiving the actual packets. Decawave DW1000 reports the estimated CIR for every received packet. If multiple packets arrive within a very short time period ($\approx$ 1 µs), their signals are visible in the CIR estimated for the first arrived packet. For simplicity, we use the same notation for responder nodes, as shown in Figure 2.5, with all responder nodes (R_1, R_2, ..., R_n)

ordered by their distance to the initiator node (I). R_1 is the closest node to I; hence, I only receives the response packet from R_1. DW1000 precisely estimates and reports the ToA for the response from R_1 by combining information from multiple estimations and interpolation components. One of these components is a leading detection algorithm (LDE), a threshold-based algorithm, which finds the CIR index corresponding to the first path of a signal. By applying a similar method to the same CIR estimate, we can find the first path corresponding to the other concurrently received signals (R_2, R_3, ..., and R_n). We can then translate the time difference between the first signal and other concurrent signals to the difference in their distance to I. We break down the design of R3 into two components. The first component enables R3 to detect concurrent responses in run-time, resilient to the impact of strong reflections and MPCs. The second component enables R3 to operate in longer distances while maintaining the accuracy of concurrent ranging.

5.2.1 Detecting Concurrent Responses

Detecting concurrent responses in run-time can be challenging, especially when they overlap with strong MPCs. When two or more signals arrive at the same time, there might be constructive or destructive interference depending on their phase difference. Concurrent ranging responses might overlap with MPCs from other responses. In our design, we take advantage of the limitation of the DW1000 chip in the resolution of TX timestamps to approach the overlapping problem. As mentioned in Section 5.1.1, $R_{i>1}$ responder signals have a larger time deviation compared to MPCs for R_1. When we look at the CIR for a sequence of packets, concurrent signal peaks are more spread over different time indices than MPC peaks for R_1. This difference in the distribution of peaks makes it possible to distinguish R_i responses from MPCs belonging to R_1. With this observation in mind, we design Algorithm 1, a concurrent response detection algorithm that makes use of a power boundary filter and a matched filter. Before using this algorithm, R3 collects CIR for N packets. Then it aligns CIR for each packet according to their first path index, reported by DW1000 chip. $DetectCR$ function takes these aligned CIRs and calculates their amplitudes. Since each CIR sample consists of I_j and Q_j components, we can calculate the amplitude of each sample using a

Algorithm 1 Concurrent Response Detection

```
Input: Threshold_Correlation, Template_ConcurrentResponse,
  CIR_Packet_1[], ..., CIR_Packet_N[]
Output: Index_ConcurrentResponse
  function MatchedFilter(Signal[], Template[])
      Signal[] ← Upsample(Signal)
      Signal[] ← Normalize(Signal)
      CrossCorrelation[] ← Signal * Template
      L ← length(Signal)
      Index_Max ← NULL
      Value_Max ← 0
      for l ← 1 to L do
          if Value_Max < CrossCorrelation[l] then
              Index_Max ← l
              Value_Max ← CrossCorrelation[l]
          end if
      end for
      return Index_Max, Value_Max
  end function
  function DetectCR(Thresh, Template[], CIR[][])
      N, M ← dim(CIR)
      Amp[][] ← CalculateAmplitudes(CIR)
      Amp[][] ← PowerBoundaryFilter(Amp)
      Amp_Max[] ← Zeros Array of Size M
      for j ← 1 to M do
          Amp_Max[j] ← max(Amp[1...N][j])
      end for
      while TRUE do
          I, V ← MatchedFilter(Amp_Max, Template)
          if V > Thresh then
              return I
          else if V = 0 then
              return NULL
          else
              Amp_Max[I] ← 0
          end if
      end while
  end function
```

Euclidean norm as $Amp_j = \sqrt{(}I_j{}^2 + Q_j{}^2)$. Then the function passes the calculated amplitudes to a *PowerBoundaryFilter* function, which subtracts a power boundary from amplitudes, calculated by Equation 5.1, based on the Friis transmission equation.

$$P[m] = Amplitude_{\mathrm{FirstPathPeak}} \times \frac{Index^2_{\mathrm{FirstPathPeak}}}{m^2} \tag{5.1}$$

After applying the power boundary filter, R3 applies a matched filter on maximum amplitude observed in each time index, by calling *MatchedFilter* function. The matched filter calculates cross-correlation between the upsampled and normalized version of the input signal and a signal template by calculating the convolution of the two signals. R3 uses a Gaussian function as a signal template, with a constant standard deviation calculated based on empirical observations. *MatchedFilter* reports index ($Index_{\mathrm{Max}}$) and value ($Value_{\mathrm{Max}}$) of the maximum calculated correlation. If the maximum correlation value is too small, it indicates the presence of a strong MPC with a larger amplitude than concurrent response. If $Value_{\mathrm{Max}}$ is below a constant pre-defined threshold, calculated based on empirical observations, R3 removes the sample at $Index_{\mathrm{Max}}$. R3 repeatedly applies the matched filter until the maximum calculated correlation exceeds the pre-defined threshold.

5.2.2 Increasing the Ranging Accuracy with Clock Skew Correction in Long Distances

Usually, a lower data rate and a longer preamble sequence increase the range at which two transceivers can communicate. Lower data rate naturally increases the communication range. However, without a longer preamble sequence, it is harder for the receiver to synchronize with the transmitter due to a lower signal-to-noise- ratio (SNR). A longer preamble makes it easier for the receiver to synchronize with the transmitter. A longer preamble makes it necessary for the devices to reply with some delay that is identical across the receiver devices. It is challenging to precisely and accurately time these delays before transmissions due to clock differences across the devices. Each responder calculates the TX timestamp by adding a constant delay, δ_{TX}, to the RX timestamp of the ranging poll message, as shown in Equation 5.2.

$$t_{\mathrm{RESP_{TX}}}[n] = t_{\mathrm{POLL_{RX}}}[n] + \delta_{\mathrm{TX}} \tag{5.2}$$

IEEE 802.15.4 UWB standard defines a ranging marker (RMARKER) as the reference for the TX and RX timestamps for two-way ranging [30]. The standard specifies the first pulse of the physical layer (PHY) header (PHR) as the RMARKER. Since the transmitter has to send the preamble sequence before the PHR, a longer preamble sequence needs a longer time period before sending the RMARKER. Consequently, responders need to increase their reply delay, giving the radio transceiver enough time to send the preamble sequence first. A larger reply delay increases the clock drift-induced error for transceivers using independent oscillators. We tackle this issue by using clock skew estimation and correction.

If each responder has an estimate for the clock skew ($\hat{\alpha}[n]$) relative to the initiator node, it can correct the clock skew by using Equation 5.3.

$$t_{\mathrm{RESP_{TX}}}[n] = t_{\mathrm{POLL_{RX}}}[n] + \delta_{\mathrm{TX}} \times (1 + \hat{\alpha}[n]) \tag{5.3}$$

According to Equation 2.11, we need to calculate the difference of two consecutive clock offset values between each responder and the initiator node. By embedding the TX timestamp in the ranging poll message and using the RX timestamp, each responder can calculate $\theta_{\mathrm{ToF}}[n]$, the relative clock offset, including the ToF, as shown in Equation 5.4.

$$\theta_{\mathrm{ToF}}[n] = \theta[n] + ToF = t_{\mathrm{POLL_{RX}}}[n] - t_{\mathrm{POLL_{TX}}}[n] \tag{5.4}$$

Since $\theta_{\mathrm{ToF}}[n] - \theta_{\mathrm{ToF}}[n-1] = \theta[n] - \theta[n-1]$, we do not need to calculate the ToF. If we assume the initiator node as the time reference, we can estimate $\tau[n]$ by using Equation 5.5. Finally, we can rewrite Equation 2.11 as Equation 5.6.

$$\tau[n] \approx t_{\mathrm{POLL_{TX}}}[n] - t_{\mathrm{POLL_{TX}}}[n-1] \tag{5.5}$$

$$\hat{\alpha}_B^A[n] = \frac{\theta_{\mathrm{ToF}}{}_B^A[n] - \theta_{\mathrm{ToF}}{}_B^A[n-1]}{t_{\mathrm{POLL_{TX}}}[n] - t_{\mathrm{POLL_{TX}}}[n-1]} \tag{5.6}$$

5.3 Evaluation

We evaluate our system by analyzing the ranging performance in terms of accuracy and precision and explore the strengths and limitations of R3.

5.3.1 Experimental Setup

In our experiments, we used Decawave TREK1000, a development kit based on DW1000 chip, as our UWB radio transceivers. We deployed all the radio nodes inside the PGH building at the University of Houston in a 23 m $\times$ 3 m corridor. As illustrated in Figure 5.4, we used one initiator node, I, and two responder nodes, R_1 and R_2. We placed R_1 in 1 m distance from I (d_1) and placed R_2 on the same line at different distances. Although all responders were in LoS with I, in most of our experiments, we observed strong reflected MPCs in CIR.

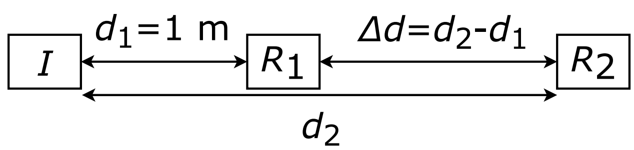

Figure 5.4: Experimental setup for the evaluation of concurrent ranging. d_1 was fixed to 1 m, while we changed d_2 for different experiments.

5.3.2 Impact of Distance on Ranging Error

We placed responder nodes at different distances to I, using the experimental setup illustrated in Figure 5.4. We verified that the distance between I and R_1 does not significantly affect the performance of concurrent ranging since the DW1000 chip itself estimates its ToA. Thus, we only used a fixed distance for R_1 ($d_1 = 1$ m). We increased d_2 from 4 m to 19 m and run Algorithm 1 for 200 packets, with the correlation threshold set to 40 and the standard deviation of the Gaussian signal template set to 10. We observed the presence of strong MPCs between 5 ns and 45 ns after the first peak (R_1), overlapping with R_2 peaks at $d_2 = 4$ m ($\Delta d = 3$ m) and $d_2 = 7$ m ($\Delta d = 6$ m), which should arrive at approximately 20 ns $\pm$ 8 ns and 40 ns $\pm$ 8 ns after R_1. Figure 5.5 shows the resulting ranging error for different d_2 distances. Ranging accuracy and precision decrease with the increase of distance, but we observe improvement for some distances due to the absence of strong MPCs after $d_2 = 7$ m. However, in longer distances with the decrease in SNR, R3 cannot easily distinguish the concurrent ranging signals from noise. These observations suggest that R3 effectively removes the impact of strong MPCs even when overlapping with concurrent ranging signals.

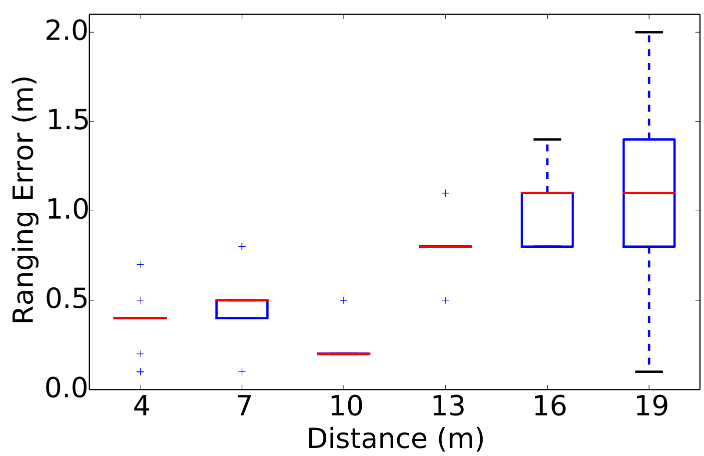

Figure 5.5: Concurrent ranging error for 200 packets as a function of d_2, the distance between I and R_2. Ranging accuracy and precision decrease in longer distances due to lower SNR. Better performance at 10 m is due to the absence of strong MPCs at that distance.

5.3.3 Number of Concurrent Ranging Rounds

We need to repeat concurrent ranging in multiple rounds to be able to analyze the distribution of the estimated ToA for $R_{i>1}$. To identify how many rounds are required, we analyze the effect of the number of concurrent ranging rounds on the ranging error, using the same experimental data and algorithm configurations as Section 5.3.2. Figure 5.6 shows that with as low as 20 rounds of ranging, we can achieve sub-meter concurrent ranging precision and accuracies better than 2 m. For longer distances, the number of ranging rounds does not improve the performance since the SNR is very low; hence it is challenging to distinguish signal from noise.

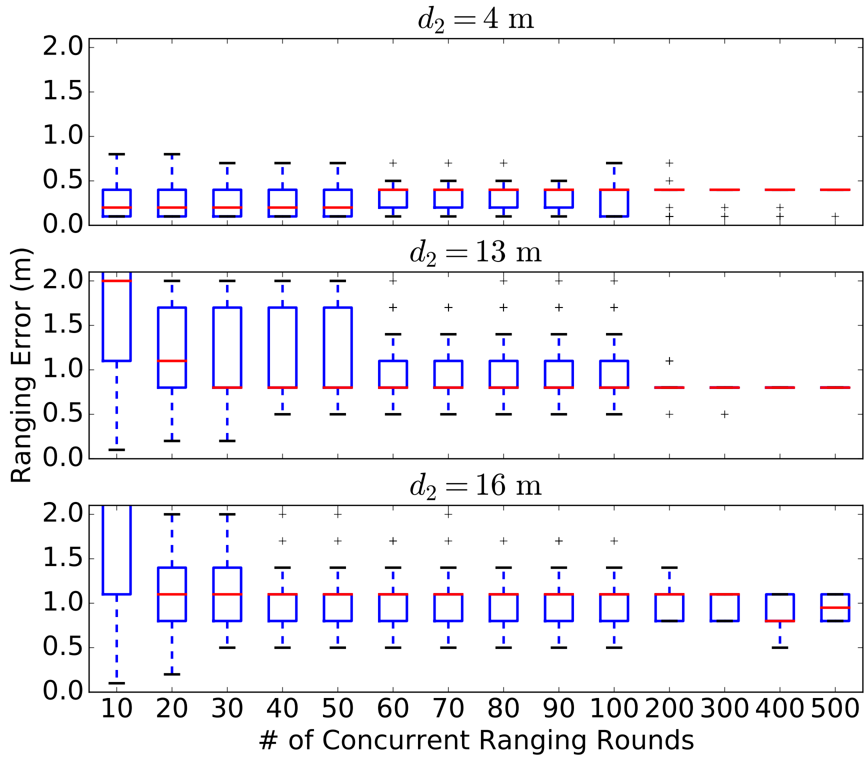

Figure 5.6: Ranging error as a function of the number of concurrent ranging rounds, for three different d_2 distances. Overall, the ranging error decreases with the increase in the number of rounds. At 16 m, the performance does not increase after 40 rounds due to low SNR.

5.3.4 Impact of Clock Skew Correction on Ranging Error

To evaluate our α correction method, we increased the response delay δ_{TX} from 800 µs to 25 ms and measured the ToA in two cases switching the α correction on and off. In Figure 5.7, we can easily see that increasing δ_{TX} to 25.3 ms increases the ranging error up to 3.76 m. When we use the α correction method, regardless of the value of δ_{TX}, the ranging error does not significantly change. For longer distance communication and ranging, we need to use the data rate of 110 kbps, which requires using a longer preamble sequence. A preamble sequence of length 4096, results in an increase of δ_{TX} to at least 4096 µs or approximately 4.1 ms. From Figure 5.7, we can see that for 4.3 ms, the ranging error is around 55 cm without α correction compared to 1 cm error with α correction. Thus, R3 improves the ranging accuracy by at least 54 cm for distances larger than 50 m. Further, the average accuracy improvement is 97.4% for all different tested response delays.

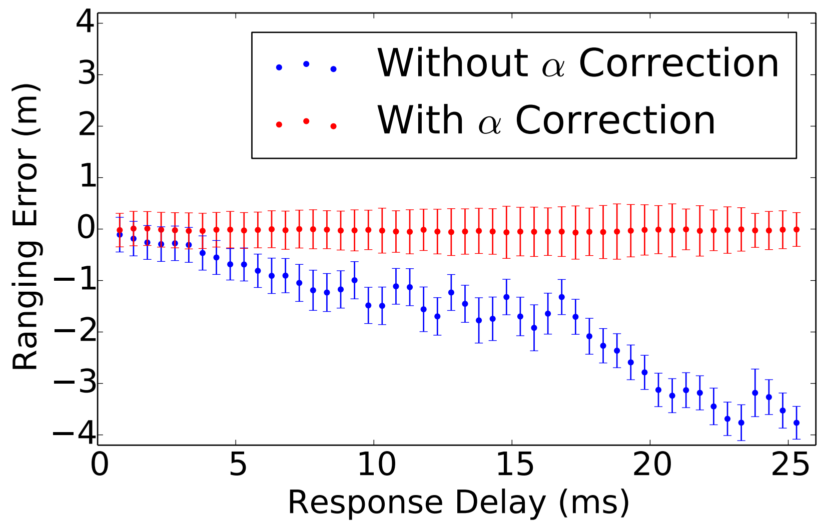

Figure 5.7: Concurrent ranging error as a function of response delay (δ_{TX}). An increase in the response delay significantly increases the error due to clock drift. When we use the clock skew (α) correction method, the error is significantly decreased, with very small jitter. Each dot represents the mean ranging error calculated for 10000 packets and error bars represent one standard deviation.

5.4 Discussion

We calculated the peak detection algorithm parameters based on empirical observations. The standard deviation of the Gaussian template represents the hardware timing uncertainty and should not change in other environments. The required number of ranging rounds and the correlation threshold depend on the number and the strength of MPCs present in the received signal. We believe our evaluation environment is representative of scenarios where strong MPCs are present. The results are likely to generalize to other real-world environments.

The design of R3 relies on the difference between ToA of the first concurrent response (from R_1)

and other responses (from $R_i > 1$). However, all other responders have the same deviation in ToA, making it hard to distinguish them from each other. We can extend the design of R3 to potentially solve this problem. After the detection of R_2 signals, we can narrow the search window down to $\pm$ 8 ns around the output index from the detection algorithm and find all peaks belonging to R_2 signals. Then we turn the problem into a similar problem by aligning the remainder of CIR with respect to the newly discovered peaks. When we align CIR with respect to the responder peaks, we accumulate the time deviation on farther responder peaks and make it possible to differentiate R_j peaks from R_{j+1} peaks. We can run the same peak detection algorithm on the newly aligned signals to discover the next closest responder.

At longer distances, with a decrease in SNR, it is harder for R3 to distinguish responder signals from noise. We can increase the TX power for farther responders to increase the SNR. Each responder can estimate the received signal level for ranging poll messages from the initiator and adaptively increase its TX power. DW1000 supports up to 33.5 dB TX power boost, with a resolution of 0.5 dB, making precise adaptive tuning of the TX power possible for each responder.

5.5 Conclusions

We designed and implemented R3, a Reflection Resilient Ranging solution, that exploits the difference in the distribution of time of arrival between first responder MPCs and other responders' signals to reliably detect concurrent responses, even in the presence of strong MPCs. R3 also makes use of the precise timing features of DW1000 to accurately estimates the clock skew between the initiator and responders to make accurate concurrent ranging feasible in distances longer than 50 m. We consider the design of R3 as a step toward a practical UWB concurrent ranging solution that can be used in real-world environments where RF multipath propagation severely impacts the quality of concurrent ranging. The results indicate that R3 can achieve sub-meter precision concurrent ranging in long distances using only a small number of ranging rounds.

Chapter 6

AnguLoc: Concurrent Angle of Arrival Estimation for Indoor Localization with UWB Radios

AoA estimation with UWB was introduced and demonstrated as a promising technology [15]. However, AoA-based localization is often neglected, especially for self-localization, due to two main technical challenges it raises. **Front-back ambiguity:** An array of antennas of size two cannot determine whether the arriving packet is received from the front of the antenna or the back. **AoA receiver unknown tilting:** AoA is always measured with respect to the plane of the antenna array. If the AoA receiver has an unknown tilting, the measured angle would be unknown.

The state-of-the-art UWB-based indoor concurrent localization systems, SnapLoc [23] and Chorus [7], implement a GPS-like system, where tag nodes estimate their location using the TDoA technique. Tags derive TDoA by estimating the ToA for concurrently received messages from multiple anchors by analyzing the combined CIR. The accuracy of location estimates depends on the accuracy of TDoA measurements. Many of the indoor localization systems, including state of the art [7, 23], have been demonstrated on the DW1000 platform. The transmission scheduling uncertainty of DW1000 introduces a jitter of approximately 8 ns, which can cause up to 2.4 m of the localization error. The state-of-the-art solution requires the reference node to transmit additional information to tags to correct their ToA estimates. This information is either transferred to the reference node through a wired backbone or transmitted with a wireless message. The latter requires estimation of error with the knowledge of antenna delays. Both of these solutions add complexity to the system and cause scalability issues.

We explore a particular design of concurrent AoA that is unaffected by this TX scheduling uncertainty in concurrent-transmitter localization systems. Our system does not use the location of the concurrently received signal peaks for time measurement. Instead, it only relies on the phase measurement on the peaks detected using signal matching because we are only interested in angle measurements. Thus, we avoid the need to estimate and correct for the transmitter scheduling uncertainties. To the best of our knowledge, the work described in this dissertation is the first demonstration of the feasibility of concurrent AoA estimation with UWB radios.

We first explore the feasibility of concurrent AoA estimation with UWB radios. Further, we introduce AnguLoc, an efficient and scalable indoor localization system based on the ADoA technique to overcome the front-back angle measurement ambiguity problem and to work with the unknown tag tilting. This algorithm has no assumptions on concurrency and can also be generalized to a sequential AoA scheme. AnguLoc utilizes concurrent AoA estimation to reduce the number of required packet exchanges. AnguLoc is four times faster than sequential AoA and improves the localization accuracy by up to 44.33% compared to state-of-the-art concurrency-based indoor localization solutions without any additional timestamp correction. AnguLoc is four times faster than sequential AoA localization systems.

In this chapter, focus on these contributions:

- Study the feasibility of concurrent AoA estimation with UWB radios and comparison with sequential AoA estimation baseline.
- Design, implementation, and evaluation of AnguLoc on Decawave PDoA node (DWM1002), which is slowly being released to the public and likely to become a major localization platform.

6.1 System Design

AnguLoc is the first system that shows how to concurrently estimate AoA. AnguLoc also provides an algorithm based on ADoA between pairs of anchors to find the location of tags.

6.1.1 Angle of Arrival Estimation Primitives

Generally, there are four ways of performing AoA estimation using multiple UWB radios: ToF, TDoA, PDoA, and TDoA/PDoA hybrid [15]. Figure 2.6 illustrates an arriving signal at an antenna array of size two. The signal travels a path difference p longer, to reach the second antenna. With an antenna separation of length d, the path difference $p = d \times \sin\theta$, where θ is defined as the angle of arrival. Time-based methods require either large antenna separation, which impacts the form factor of self-localizing tags, or extremely precise ToA estimation. Decawave DW1000 radio has a precision of 333 ps or equivalently 10 cm [10], which requires an antenna separation of at least $d = 1.14$ m for an angle of arrival precision of 5°. However, the precision of the PDoA method depends on the carrier frequency and antenna separation. The drawback of the PDoA method is the requirement of highly precise phase synchronization between the two radios. One way to address this issue is to clock the two radios from the same frequency oscillator.

6.1.1.1 Mapping Phase Difference of Arrival to Angle of Arrival

We can calculate PDoA by taking the difference between individually calculated phase by each radio and mapping the PDoA to AoA. DW1000 reports CIR as a sequence of I and Q samples, representing the real and imaginary parts of each CIR sample. We can calculate the phase of arrival (PoA) of the preamble for each radio as $\arctan \frac{Q_i}{I_i}$, with i being the sample number, which DW1000 reports as the first path of the signal. Further, Decawave suggests a phase correction by deducting the start of frame delimiter (SFD) phase from the calculated PoA. Finally, PDoA (α) is the difference between corrected PoA values of each radio, mapped to $[-\pi, \pi]$. With a wavelength of λ, $p = \frac{\alpha \times \lambda}{2\pi}$. Solving for θ gives us $\theta = \arcsin \frac{\alpha\lambda}{2\pi d}$. To have a one-to-one mapping between α and θ, the antenna separation of d needs to be less than half of the wavelength ($\frac{\lambda}{2}$). Details of AoA estimation are also available in Decawave's patent [45].

6.1.1.2 Antenna Modification for Receiving from Front and Back

AnguLoc builds a localization system that relies on the reception of packets from all directions. The antenna designed for DWM1002 is a directional antenna that receives with a reasonable quality only from one side. To address this issue, we disconnected the antenna from DWM1002 and attached two Decawave dipole antennas. We separated the two antennas by a distance of approximately 3.75 cm, which is half the wavelength for the 4 GHz frequency channel.

6.1.1.3 Calibration and Correction for Antenna Characteristics

With a centimeter-level wavelength, the path difference p causes a large PDoA (α). Any asymmetry in the design of the antenna paths would cause a large difference in the phase difference at both antennas, even with an angle of 0°. For example, with the 2 cm antenna separation for 6.5 GHz frequency channel, 1 mm of asymmetry would translate to an error of $\arcsin \frac{0.001}{0.02} = 2.8°$. We need to calibrate each board separately for such errors by measuring the PDoA error at 0° and correcting the PDoA in later measurements.

With antenna separation smaller than a few wavelengths, they interact with mutual coupling, which causes the effective path difference to be different from the geometric path difference [8]. Since this behavior is non-linear, we use a polynomial correction function. By measuring at multiple samples at different angles, we fit a polynomial that corrects for the antenna characteristics. For our customized antenna, we use the following polynomial to correct the path difference p:

$$12600.13p^4 - 575.45p^3 - 12.40p^2 + 1.56p + 0 \tag{6.1}$$

6.1.2 Concurrent Angle of Arrival Estimation

Concurrent AoA estimation combines the idea of AoA estimation on UWB radios with concurrent transmissions.

6.1.2.1 Channel Impulse Response and the Concurrency Window

CIR is obtained by accumulating cross-correlation values between the arriving stream of repeated preamble sequence and a known sequence. When preambles of multiple packets arrive at a receiver, only if they arrive in a short time window after the first packet, the correlation would be large at multiple points in CIR, showing multiple CIR peaks. We call this time window the *concurrency window*. The length of CIR is a maximum of 1016 ns, but in practice, we observed that we could only use approximately half of the CIR length as the *concurrency window*. Beyond that, the receiver cannot differentiate between the second arriving signal and the first arriving signal. In that case, either the receiver synchronizes with the second arriving signal, or it cannot synchronize with any of the arriving signals. Figure 6.1 shows CIR estimates for five packets arriving at two receivers in a *concurrency window*.

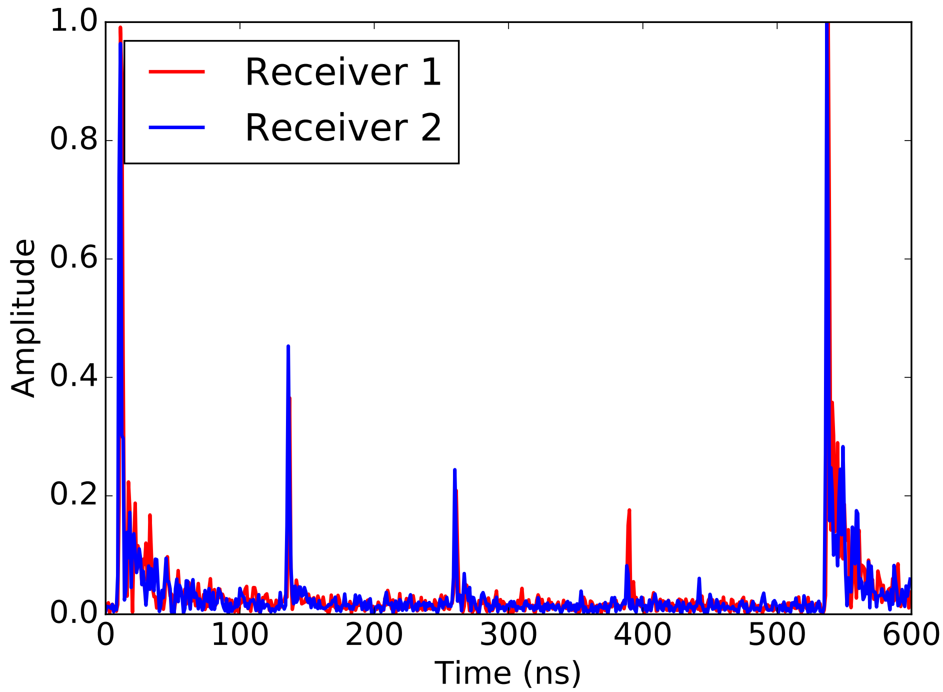

Figure 6.1: CIR estimated at the PDoA node when receiving concurrently from five responders. CIR is well aligned for all responses in both receiver nodes.

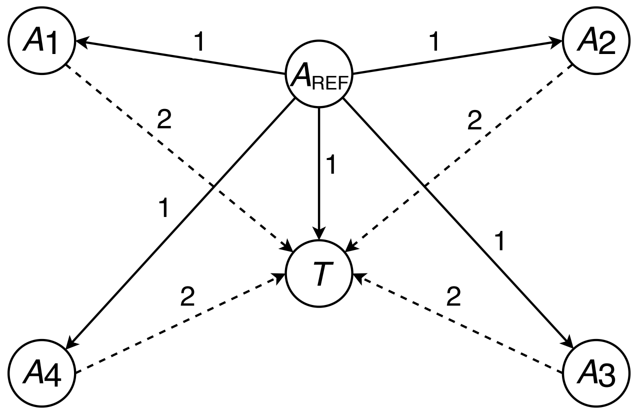

Figure 6.2: Illustration of concurrent transmissions protocol for localization. First, A_{REF} broadcasts a *SYNC* packet (shown with number 1). Upon reception of *SYNC*, all anchors (A_i) broadcast a *REPLY* packet (shown with number 2). All *REPLY* packets arrive at the Tag (T) (quasi-)simultaneously.

6.1.2.2 Responder Synchronization Protocol

One method to achieve concurrent transmissions and receive all responses in a *concurrency window* is to synchronize multiple transmitters with a *SYNC* packet. As depicted in Figure 6.2, all responders (anchors for localization) broadcast a *REPLY* packet when they receive the *SYNC* packet. Adding a time delay ΔR to the ToA of the *SYNC* packet helps to remove most of the system-level jitters. Finally, tags receive *REPLY* packets (quasi-)simultaneously. State-of-the-art concurrent localization systems [7, 23] suggest using a response position modulation. This solution resolves issues of the overlapping responses with MPCs, and overlapping responses of the equidistant transmitters. The response position modulation is implemented by deliberately adding specific delays (δt_i) in response, in addition to the already existing response delay (ΔR). With enough delay set for δt_i, we increase the probability of peak detection since MPCs decay in further CIR samples. With the assumption of a maximum distance between transmitters, the response position modulation also helps with the problem of equidistant nodes. Similar to the state of the art, we define $\delta t_i = (i - 1) \times \alpha$, where i is the node ID, and α is set to 128 ns. Because of clock drift between responders, if we increase ΔR, the position of peak might shift in time. For $\Delta R = 25$ ms this shift goes up to 12 ns [27]. This shift in time affects the performance of response position modulation and its robustness against MPCs. We use the same time synchronization methodology used by the state of the art to avoid this problem [23, 27].

6.1.2.3 Detection and Extraction of Concurrent Response Peaks

Similar to concurrent localization systems, concurrent AoA estimation relies on reliable detection of concurrent responses. Without a reliable peak detection, we might misclassify noise, MPCs, and concurrent peaks. State-of-the-art concurrent localization systems suggest using a search and subtract (SS) algorithm to reliably find the concurrent peaks [7,23]. We also adopt the SS algorithm for reliable peak detection as follows. We first extract a pulse shape for PG_DELAY of 0x95 for frequency channel 4 by transmitting packets in a noise-free environment and recording the first path of CIR and averaging them for 1000 packets. We use this pulse shape as our signal template. To detect if there is any peak from a responder and avoid detecting noise, we only consider the peak if it has an amplitude exceeding a noise threshold, $\eta = 12 \times \sigma_{\text{noise}}$ [7]. The SS algorithm is as follows:

(i) Divide the CIR into multiple chunks with respect to the 128 ns delays set for each responder. The size of each window is 128 ns, centered around the position of each responder. The first window starts at 64 ns after the first peak.

(ii) Upsample each CIR chunk using FFT with the upsampling factor set to $L = 30$.

(iii) Normalize the upsampled CIR chunk.

(iv) Cross-correlate the chunk with the signal template and find the index with maximum correlation.

(v) If the sample at the found index has an amplitude exceeding a noise threshold, $\eta = 12 \times \sigma_{\text{noise}}$, we consider it as a concurrent peak.

6.1.2.4 Angle of Arrival Estimation for Multiple Responders

We fuse the information we extract from the CIR of the two radios to calculate AoA for each concurrent response using Algorithm 2. The inputs of the algorithm are the maximum number of concurrent responses expected, CIR from the first radio, and CIR from the second radio. $FindPeaks$ is the function that extracts concurrent peaks using the method described in Section 6.1.2.3. $Peaks$ is a 2D array containing the time sample index indicating the presence of each peak. Finally, we feed the found peak pairs from both radios belonging to each concurrent response to $CalcAoA$, the AoA calculation function described in Section 6.1.1.1, to calculate and output the concurrent AoA estimates.

Algorithm 2 Concurrent AoA Estimation

Input: $MaxNumResponses, CIR_1[], CIR_2[]$
Output: $AoA[]$
  $N \leftarrow MaxNumResponses$
  $Peaks[1 \ldots N][1] \leftarrow FindPeaks(N, CIR_1[])$
  $Peaks[1 \ldots N][2] \leftarrow FindPeaks(N, CIR_2[])$
  for $i \leftarrow 1$ to N **do**
    $AoA[i] \leftarrow CalcAoA(Peaks[i][1,2], CIR_1[], CIR_2[])$
  end for

6.1.3 Concurrent AoA vs. Concurrent TDoA

We compare concurrent AoA estimation systems with concurrent TDoA systems to understand concurrent AoA (what we propose) with respect to concurrent TDoA (which has been discussed in the literature).

6.1.3.1 Fusing Information from Multiple Radios

For AoA estimation, we need a receiver with multiple radios to measure the phase on different antennas and combine them to estimate AoA. Doing such measurements requires that the radios are synchronized in phase. Clocking radios from the same crystal oscillator helps synchronize the phase, but it also requires careful design of the hardware. To ensure phase synchronization, we need to minimize any asymmetry in the board in both antenna path and clock path. For TDoA estimation, we need a receiver with one radio, which makes the design of the hardware simpler.

6.1.3.2 Working with Phase instead of Time

For AoA estimation, we need to work with phase information rather than time information, which is used by TDoA estimation. The main advantage of working with phase information is the immunity against time scheduling uncertainties and jitters in the transmitters. TDoA systems rely on the difference in ToA for packets from multiple transmitters. Concurrent TDoA systems rely on synchronized transmissions. Hence, any jitter or scheduling uncertainties affect their performance negatively. The jitters do not impact concurrent AoA estimation systems at the transmitters since we only work with the PDoA at the receiver for each transmitter. Hence, concurrent AoA systems are immune to timing jitters.

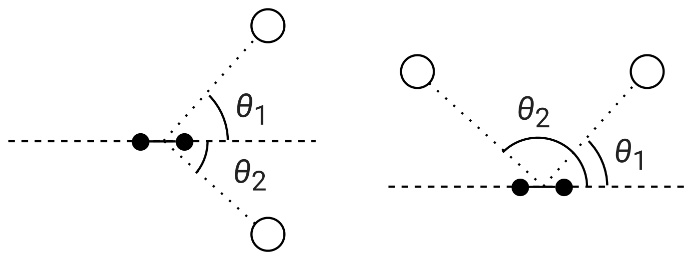

(a) $\theta_{1,2} = \theta_1 + \theta_2$ (b) $\theta_{1,2} = |\theta_1 - \theta_2|$

Figure 6.3: Two different cases of *tag antenna plane* for computation of the angle difference between a tag and a pair of anchors.

6.1.4 Angular Localization Algorithm

AnguLoc uses angle differences between pairs of anchors for localization and is considered as an ADoA algorithm. AnguLoc extends the ADoA algorithm [71] to address the front-back ambiguity issue. We assume nothing about the concurrency; hence, our algorithm is also generalizable to sequential AoA. We assume N anchors positioned at $A_i = (x_i, y_i)$ $(1 \leq i \leq N)$, and a tag having unknown angle θ and position $T = (x, y)$. In the case of known tag tilting, at least three anchors are required to find the tag position, since there are only two angle differences for three anchors and we have two unknowns (x, y). For the case of unknown tag tilting, we need $N \geq 4$. Suppose the line segment connecting i^{th} and j^{th} anchors subtends angle difference $\theta_{i,j}$ from the tag. Regarding tag and these two anchors, there are two different possibilities, as illustrated in Figure 6.3. The first possibility is that the *tag antenna plane* and the passing line segment intersect. The second possibility is that they do not intersect. In the first case, $\theta_{i,j} = \theta_1 + \theta_2$ and in the second case $\theta_{i,j} = |\theta_1 - \theta_2|$. Since we have front-back ambiguity for angle measurements, we cannot identify which case is correct if we do not know the tag tilting. But, with the assumption that we know which scenario happens for all pairs of anchors, $\theta_{i,j}$ values are known up to a white Gaussian noise. We denote these measured noisy angles $\hat{\theta}_{i,j}$. On the other hand, the exact angles must be:

$$\theta_{i,j} = \arccos\left(\frac{TA_i \cdot TA_j}{|TA_i||TA_j|}\right) = \arccos\left(\frac{(x-x_i)(x-x_j)+(y-y_i)(y-y_j)}{\sqrt{((x-x_i)^2+(y-y_i)^2)((x-x_j)^2+(y-y_j)^2)}}\right) \quad (6.2)$$

where TA_i and TA_j are vectors from tag to anchors i and j, and $\cdot$ is the inner product operation. Therefore, one can define the following least square cost function:

$$J(x, y) = \sum_{j>i} (\theta_{i,j} - \hat{\theta}_{i,j})^2 \quad (6.3)$$

Finally, the position can be estimated as:

$$\hat{T} = \underset{x,y}{\operatorname{argmin}}\, J(x, y) \quad (6.4)$$

As illustrated in Figure 6.4, with four anchors, there are only six possible cases for *tag antenna plane*, depending on the tag tilting. First, AnguLoc finds the optimum solution $\hat{T}(x, y)$ for Eq. 6.4 for all six different cases. Then, AnguLoc chooses the solution where the residual value of $J(x, y)$ is minimum among the six cases. To find each $\hat{T}(x, y)$, we use the quasi-Newton method [57] with an initial position estimate at the center of the room. To see the typical performance of the algorithm, we use simulation. We chose 10 random tag locations in a 5 m $\times$ 5 m room with four anchors

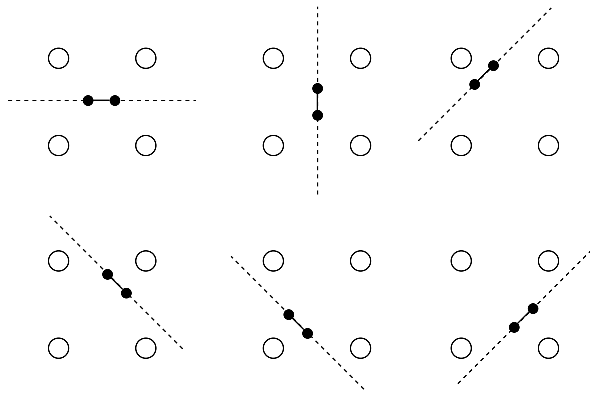

Figure 6.4: Six different cases of *tag antenna plane* for computation of angle difference in a four-anchor setting.

placed in the corners. For each tag location, we chose 20 random tag tilting uniformly spread over the interval of $[0^\circ, 360^\circ]$. For each tag location and tilting, we repeated the simulation 10 times and added random noise each time to the angle measurements. For each resulting simulated noisy measurement, we run the ADoA-based algorithm and record the residual error as the Euclidean distance between the ground truth and estimated location. Figure 6.5 shows the CDF of error for different standard deviations of noise from 2.5° to 10°. For noise levels below 5°, we can say that the algorithm has a sub-meter error 80% of the time.

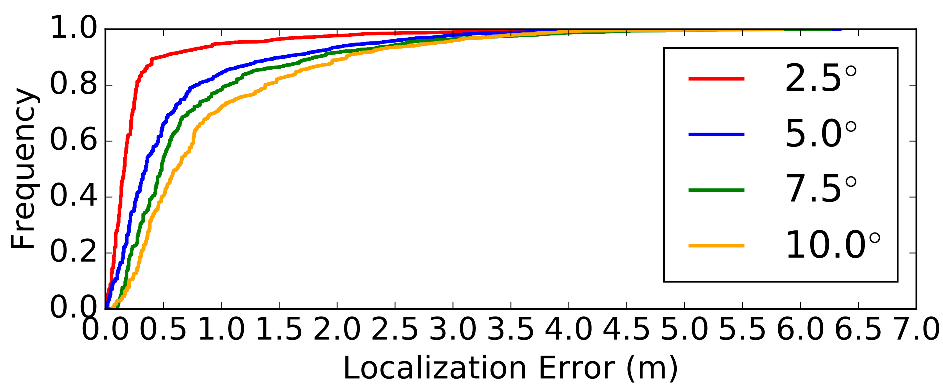

Figure 6.5: A typical performance of our ADoA algorithm simulated for different levels of angle measurement noise. The localization error is below 1 m in 80% of the time for noise levels below 5°.

6.2 Evaluation

6.2.1 Experimental Setup

In our experiments, we used Decawave PDoA Node DWM1002 (Figure 2.6) as our tag, with the modified antennas to receive from both sides. For responders/anchors, we used the radinoL4 DW1000 platform. We set up our system in the PGH building hallway of size 20 m $\times$ 3 m for concurrent AoA evaluation experiments and inside a room of size 6.5 m $\times$ 4.5 m for localization experiments. In all experiments, we placed all the nodes on tripods at 1.5 m height. We used frequency channel 4, with a preamble length of 64, a pulse repetition frequency (PRF) of 64 MHz, and a data rate of 6.8 Mbps.

6.2.2 Feasibility of Concurrent AoA

We placed the DWM1002 node in a fixed position and measured the AoA in different angles by placing the responder nodes in various angles and distances, as illustrated in Figure 6.6. The ground truth angle, θ, is the angle between the transmitter and center of the receiver antennas.

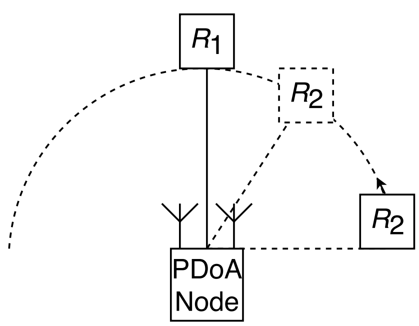

(a) Different angles

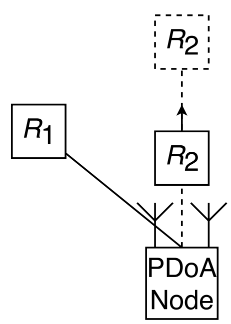

(b) Different distances

Figure 6.6: Experimental setup for the evaluation of concurrent AoA.

6.2.2.1 Platform AoA Estimation Baseline

We use a single-responder setting with DWM1002 in AoA estimation for different angles and distances as the baseline. In addition to the specifics of AnguLoc, this dissertation is also the first

Table 6.1: AoA Estimation Baseline Performance

(a) Angles

θ (°)	AoA Error (°)			
	Avg	**Std**	**50th**	**90th**
-90	0.63	2.60	0.00	0.00
-60	4.56	3.38	3.86	8.69
-30	2.42	1.81	2.07	4.82
0	3.24	2.21	2.73	6.52
30	3.20	2.46	2.59	6.44
60	4.89	3.31	4.19	9.52
90	0.51	2.77	0.00	0.00

(b) Distances

d (m)	AoA Error (°)			
	Avg	**Std**	**50th**	**90th**
3	2.12	1.63	1.65	4.51
6	2.29	1.72	1.92	4.73
9	2.52	1.85	2.26	5.01
12	2.41	1.75	2.01	4.90
15	3.30	2.49	2.83	6.24

research to evaluate the performance of DWM1002. Table 6.1 shows the baseline AoA estimation performance. AoA estimation has an error of less than 10° in 90% of the time for all angles. The antenna path correction polynomial (discussed in Section 6.1.1.3) compresses all the measurements near the antenna edges to 90° and -90°, and we get almost 0° error in 90% of the time. However, if the transmitter is not facing the receiver at the antenna edges, we get higher errors. For the distance increment experiment (Figure 6.6b), we placed the responder node at 20° and increased its distance. Table 6.1b shows that the AoA error increase by increasing the distance because of the negative effects of path loss on performance.

6.2.2.2 Concurrent AoA in Different Angles

To evaluate concurrent AoA estimation, we fix R_1 at 0° and rotate R_2 (Figure 6.6a) and measure angles for both nodes concurrently. Figure 6.7a compares the ground truth angle with the estimated AoA for R_2 concurrently, while showing the results of baseline AoA experiments. Table 6.2 compares the performance of concurrent AoA for both R_1 and R_2. Results are comparable with baseline AoA estimation performance. We also switched R_1 and R_2 and observed similar results. 0° errors are due to compression of measurements near the antenna edges to -90° and 90° by path correction polynomial. We can conclude that the concurrency does not significantly affect the AoA estimation.

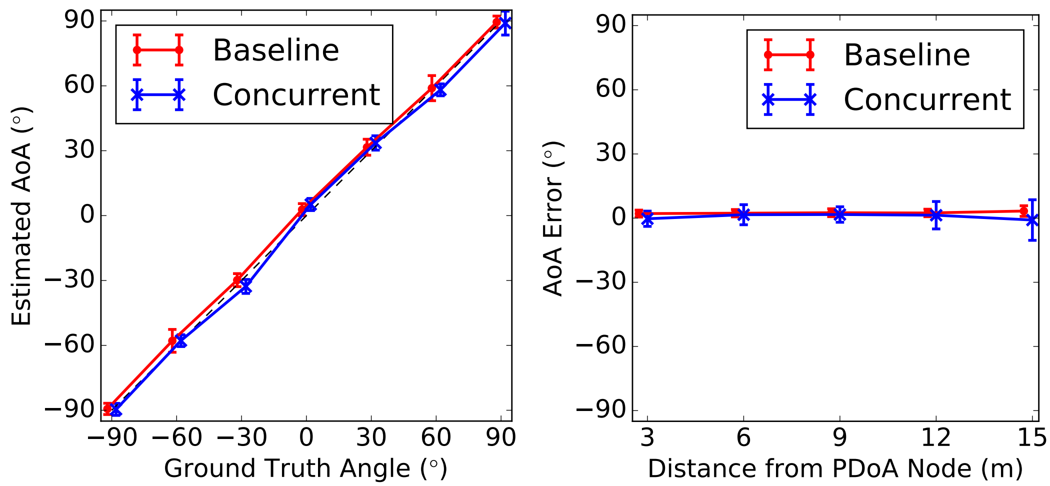

(a) Concurrent AoA in different angles.

(b) Concurrent AoA in different distances.

Figure 6.7: Evaluation of concurrent AoA estimation. Concurrency does not impact the quality of AoA estimation. Each point represents the mean value for 100 measurements and error bars are one standard deviation.

6.2.2.3 Concurrent AoA in Different Distances

We fix R_1 at 30°, move R_2 away at 0° (Figure 6.6b), and measure angles for both nodes concurrently. Figure 6.7b compares the concurrent AoA error in different distances for R_2 while showing the results of baseline AoA experiments. At distances beyond 12 m, the path loss for the farther node decreases the performance, since the concurrent peak size shrinks. Table 6.3 compares the performance of concurrent AoA for both R_1 and R_2. Results are comparable with baseline AoA estimation performance. We also switched R_1 and R_2 and observed similar results. In this case, at longer distances of R_1, the path loss for R_1 is much higher than R_2, causing failure to receive the packet from R_1. We can conclude that the concurrency does not significantly affect the AoA estimation in small distances.

Table 6.2: Concurrent AoA Performance – Angles

θ_2 (°)	R_1 **AoA Error (°)**				R_2 **AoA Error (°)**			
	Avg	**Std**	**50th**	**90th**	**Avg**	**Std**	**50th**	**90th**
-90	3.29	2.37	2.74	5.97	0.40	2.07	0.00	0.00
-60	3.39	2.38	3.06	6.53	6.68	4.40	6.26	12.52
-30	4.23	2.66	4.09	7.53	3.76	3.20	2.51	8.73
0	5.10	2.56	5.34	8.25	5.18	2.46	5.22	8.54
30	4.03	2.76	3.77	7.48	4.56	3.90	3.29	10.29
60	4.01	2.44	3.99	7.41	5.53	4.17	5.02	11.71
90	3.23	5.24	2.32	6.15	1.00	3.45	0.00	1.68

Table 6.3: Concurrent AoA Performance – Distances

d_2 **(m)**	R_1 **AoA Error (°)**				R_2 **AoA Error (°)**			
	Avg	**Std**	**50th**	**90th**	**Avg**	**Std**	**50th**	**90th**
3	3.15	2.12	2.90	5.75	2.86	2.15	2.32	5.86
6	2.61	1.64	2.44	5.15	3.61	3.40	2.57	8.41
9	2.71	1.73	2.42	4.82	3.09	2.53	2.42	6.17
12	2.72	2.07	2.27	5.48	5.17	4.02	4.24	11.84
15	2.76	2.04	2.65	5.55	8.37	4.57	9.21	14.12

6.2.2.4 Scaling the System Beyond Two Responders

We investigate how adding more responders affect the quality of AoA estimation for each responder. For this purpose, we added more responders to the network over time. Figure 6.8 shows the AoA error, combined from concurrent AoA measurements from all responders present in the network. We observe that the error does not increase by adding more responders up to 5 nodes. When we add more responders to the network, we cannot receive most of the packets from the first responder. When a concurrent peak is more than half a preamble symbol away from the first responder, it is hard for the receiver to distinguish which of the responders' signals arrived first. In this case, we receive the packet from the last responder instead.

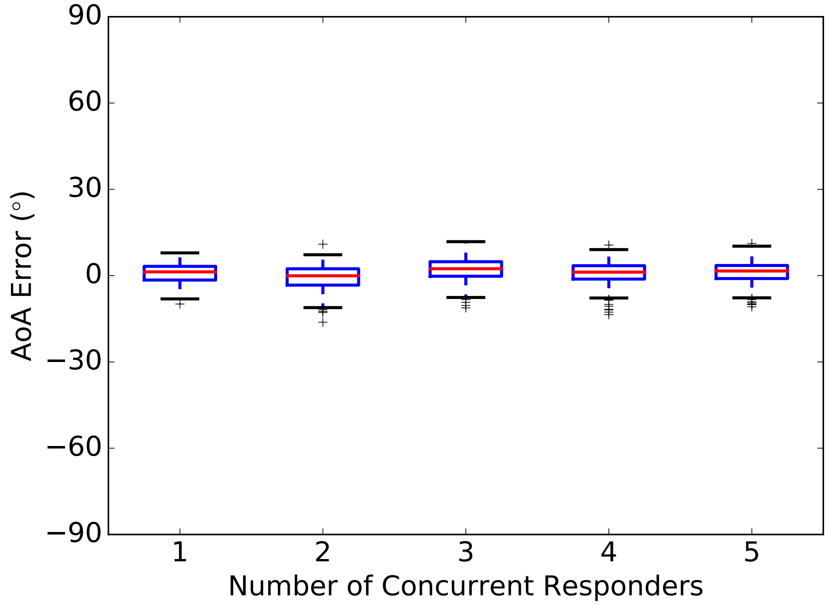

Figure 6.8: AoA error as a function of the number of concurrent responders in the network. Each box plot represents combined errors from all nodes present in the network for 100 measurements.

6.2.3 Indoor Localization with AnguLoc

We placed four anchors in the corners of a room, more specifically at (0 m, 0 m), (3 m, 0 m), (0 m, 6 m), and (3 m, 6 m). To see the performance of AnguLoc, we first placed our tag node at 10 different locations in the room, at angles of 0°, 45°, and 90°. For each setting, we collected more than 100 data points, resulting in a total of 3000 location estimates. Second, we collected data for a mobile tag moving in the room on a rectangular shape path, 50 cm away from the borders. We moved the tag at a constant speed to make it easier to approximate the ground truth. For the mobile setting, we collected more than 200 data points. We run AnguLoc on the collected data, as well as state-of-the-art concurrent TDoA algorithm for comparison. We did not implement timestamp correction methods suggested by SnapLoc [23]. Figure 6.9 shows the CDF of localization error for both static and mobile experiments, comparing AnguLoc and concurrent TDoA (CTDoA) method. In the static setting, the 90th percentile of error for AnguLoc is 0.67 m, and for CTDoA is 1.20 m. In the mobile setting, the 90th percentile of error for AnguLoc is 1.11 m, while it is 1.41 m for CTDoA. AnguLoc improves the localization accuracy by 44.33% in the static setting and by 21.46% in the mobile setting, compared to the CTDoA method without timestamp correction. AnguLoc takes more time than CTDoA to estimate the location since it has to solve six optimization problems to consider every tag tilting possibilities.

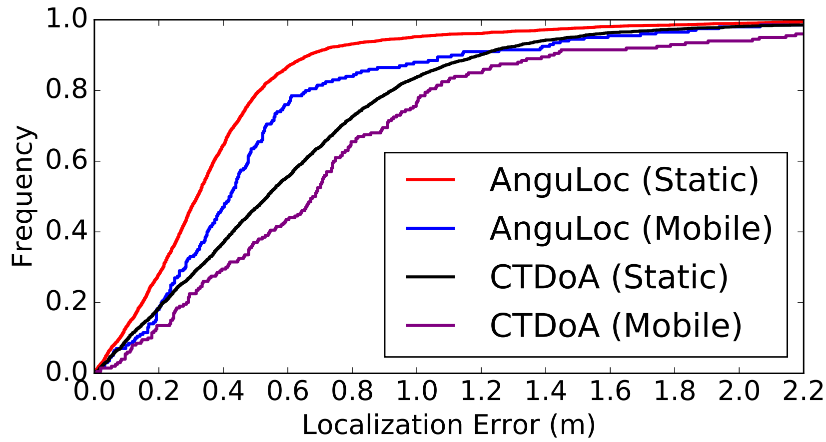

Figure 6.9: CDF of localization error for AnguLoc and concurrent TDoA, with static and mobile tag. CDF for static tags is aggregated for more than 3000 location estimates. CDF for mobile tags is aggregated for more than 200 location estimates. AnguLoc outperforms concurrent TDoA method.

6.3 Discussion

6.3.1 Angular Localization Algorithm in Sequential Localization Schemes

In this work, we propose an angular localization algorithm based on the ADoA technique (Section 6.1.4). AnguLoc uses that algorithm in a concurrent transmission setting. The localization algorithm itself does not rely on concurrent transmissions. Inputs of the localization algorithm are locations of anchors and measured angles from the tag with each anchor. This means that we can use the same localization algorithm (without any change) with a sequential transmission protocol, where each tag measures angle with each anchor one by one. Generally, the accuracy of AoA measurements is slightly better when we use sequential transmissions. However, there are some cases in which we need a faster update rate that sequential transmission protocols cannot provide. Because of the independence between the transmission protocol and the localization algorithm, using a different transmission protocol does not affect the efficiency nor the update rate of the angular localization algorithm. However, it can alter the overall update rate of the localization system by affecting the efficiency of each angle measurement. Using concurrent transmissions increases efficiency and provides a faster update rate of the overall localization system.

6.3.2 Limitations

AnguLoc has a few limitations inherited from the base solutions it is built on:

Scaling Concurrent Transmissions: Current concurrent transmission systems do not scale beyond a handful of anchors. In the case of more radio nodes, we can make multiple groups of concurrent nodes. We can assign a timeslot to each group. All nodes in one group respond (quasi-)simultaneously in the timeslot assigned to their group.

Angle of Arrival Estimation: (1) The weaker reception on the sides of dipole antennas causes a larger AoA error. (2) With the increase in distance, the performance of concurrent AoA decreases due to lower SNR. One solution is to increase the density of anchors and select the nearest anchors for localization.

6.4 Conclusions

AnguLoc is the first concurrent AoA system on UWB radios. We showed that concurrent AoA can be used with a small yet sufficient number of concurrent transmitters without performance degradation compared to sequential AoA. AnguLoc enables efficient, accurate, and scalable indoor localization. Our ADoA-based localization algorithm overcomes the front-back angle measurement ambiguity problem, which uncovers the neglected capabilities of AoA-based localization. Facilitating self-localization in AoA-based systems increases scalability to an unlimited number of tags.

Further, equipping such systems with concurrent AoA measurement capability increases the efficiency without loss of accuracy. AnguLoc is four times faster than sequential AoA when using four anchors while maintaining a sub-meter accuracy and supporting an unlimited number of tags.

Chapter 7

Future Directions

In this chapter, we discuss open research problems in concurrency-based localization, future directions, and possible continuation of our work.

7.1 Increasing the Accuracy of Concurrent TDoA Localization Systems

One advantage of concurrent TDoA that makes it a more favorable solution compared to concurrent AoA is the simpler hardware requirements. However, concurrent TDoA systems are susceptible to timing jitters that can affect their location estimation accuracy. In current concurrent localization systems, responders (concurrent transmitters) synchronize and schedule their transmission referenced to the RX timestamp of a broadcast $SYNC$ message from a reference node. In cases where the resolution of TX scheduling timestamp is lower than the RX timestamp, we lose a certain amount of timing precision. The reason is that the calculated TX timestamp has a higher resolution compared to the TX timestamp that we can use to schedule the transmission. The UWB radio ignores a certain number of lower bits in the calculated TX timestamp. The loss of precision in TX timestamp causes jitter in the transmission time for each responder. The signals arriving at the concurrent receiver then have jitter in ToA, which ultimately impact the localization accuracy.

For DW1000 radio, the TX scheduling uncertainty can cause up to 2.4 m of the localization error.

Researchers have proposed preliminary solutions [23]: (1) Transmitting the information about the lost precision to the receiver through a wired backbone, so the concurrent receiver can correct the error, (2) estimating the jitter in the reference node by comparing calculated ToF and the expected ToF (known distances), and sending this information with the next $SYNC$ message so that the concurrent receiver can correct the error. These solutions are either not practical in real-world scenarios or incur a delay in location estimation.

Another potential solution is to make the lost precision the same across all responders, so the actual transmissions have a minimum jitter relative to each other. We can achieve this by making the bits that the UWB radio ignores, the same for all responders. The key idea is to exploit the relative clocks drift between all responders. Since each of the concurrent transmitters count the time at different rates, when we add a specific delay to their TX timestamp (response delay), they transmit at different times. State of the art uses a clock skew correction method to calculate the delay with respect to a reference clock so that all concurrent transmitters transmit at the same time [23, 25, 27]. We can use a similar clock skew correction method in our solution. The goal is to find a specific delay so that when corrected for each clock, they have the same lower bits. This way, when the UWB radio ignores the lower bits, it would have the same effect for all responders. However, we still rely on the CIR for ToA estimation. Hence, the upper limit for the precision is approximately 1 ns or equivalently 30 cm.

7.2 Increasing the Scalability of Number of Concurrent Transmitters

Current concurrent localization systems use CIR to estimate ToA or PDoA of concurrent signals. The upper limit for the number of concurrent transmitters to arrive in a *concurrency window* is the length of CIR. We observed that in practice, we could use half of the CIR. With the approximately 1 ns resolution of the CIR, we can go up to 508 transmitters. However, a number of issues affect the robustness of concurrent localization systems: (1) identification of concurrent nodes, (2) overlapping responses from equidistant nodes, and (3) the overlapping of responses with strong multipath.

The related work in this area suggests using a response position modulation to address the mentioned problems above [7,23,25]. However, this solution severely degrades the scalability of the number of concurrent transmitters. Similar to the state of the art, we observed that when we use the response position modulation with 128 ns separation and we increase the number of concurrent nodes beyond five, we cannot receive concurrent packets. The limited capacity of the *concurrency window* imposes a trade-off between the scalability of concurrent transmitters and the robustness of the concurrency-based localization systems. In real-world scenarios, it may be desirable to go beyond five nodes.

One way to increase the number of concurrent transmitters without sacrificing the robustness is to use a TDMA scheme. We can make multiple groups of concurrent transmitters and assign a timeslot to each group. All nodes in one group can still utilize concurrent transmissions and respond (quasi-)simultaneously in the timeslot assigned to their group.

7.3 Increasing the Resilience of Concurrency-based Localization Against Strong Multipath

Current concurrent localization systems rely on the ability of the system to detect concurrent peaks. In the presence of strong multipath, it is hard to distinguish concurrent peaks from MPCs. We showed how using the reflection-resilient concurrent ranging (R3) developed in this dissertation can increase the ability of concurrency-based localization systems to detect concurrent peaks in case of overlapping with strong multipath. However, there are cases where even R3 cannot effectively detect peaks due to destructive interference caused by strong MPCs. In the case of dynamic environments, the MPCs can often interfere with concurrent peaks with very large amplitudes and bury the concurrent signals in noise. Another case is when there are more concurrent nodes in the network, responders' signals can overlap with each other.

The related work in this area suggests using a response position modulation to address the issue of overlapping concurrent peaks with MPCs [7,23,25]. However, this solution severely degrades the scalability of the number of concurrent transmitters.

One potential solution to increase the resilience of concurrent localization against strong MPCs is to increase the TX scheduling uncertainty by deliberately ignoring lower bits from timestamp variables and lowering the resolution of timestamps used for scheduling transmissions. This way, we can increase the deviation of time of arrival of concurrent peaks and make a wider Gaussian distribution, which makes it easier to distinguish such peaks from strong multipath.

Chapter 8

Conclusions

In this dissertation, we identified several critical issues in the existing UWB-based indoor localization systems. Those issues impact the ability of such systems to scale while maintaining efficiency and accuracy. We also identified a lack of a proper evaluation standard to compare results from different UWB-based localization studies in NLoS scenarios. Further, we provided techniques to address these issues to build scalable, efficient, and accurate localization systems and took the first step in making a benchmarking standard for UWB-based localization systems.

8.1 Summary of Contributions

In this dissertation, we made the following contributions:

Benchmarking Standard for UWB-based Localization Systems: We presented a technique to separately observe the effects of signal attenuation/refraction and diffraction. We studied the effects of these phenomena on UWB ranging for different construction materials. It is essential to take into account the types of materials used in a testing environment for proper benchmarking of different localization solutions in different scenarios.

Resilience to Strong Multipath for Concurrent Ranging: We increased the scalability of concurrent ranging by designing an algorithm to detect concurrent responses with resilience to strong multipath. We further used a clock skew correction method to reduce the concurrent ranging error induced by the clock drift in longer ranges. Our technique achieves sub-meter precision concurrent ranging and reduces the error by at least 54 cm in long distances (> 50 m) and by more than 97% on average when the ranging response delay is arbitrarily large.

Indoor Localization with Concurrent Angle Difference of Arrival: We investigated the feasibility of concurrent AoA estimation with UWB radios. Concurrent AoA is unaffected by transmission scheduling uncertainties, which ultimately increases the accuracy of concurrency-based localization systems. We further presented a localization algorithm based on the ADoA technique that addresses the front-back ambiguity and unknown device tilting issues. Our method is four times faster than sequential AoA and improves the localization accuracy by up to 44.33% compared to state-of-the-art concurrency-based indoor localization solutions without relying on additional timestamp correction.

Scalable and Efficient Concurrency-based UWB Indoor Localization: In summary, our work explores the neglected aspects of UWB-based indoor localization techniques. Lack of proper media access control in UWB networks limits the scalability and efficiency of UWB-based localization systems. By exploiting wireless interference and utilizing concurrent transmissions, we addressed the problem of scalability and efficiency while maintaining the required accuracy by many indoor localization applications. A localization system with the combination of our proposed methods (1) improves the scalability of tags to an unlimited number of tags; (2) improves efficiency by allowing concurrent transmissions and achieving fast location update rate; and (3) improves the accuracy of concurrency-based localization with a reflection resilient concurrent peak detection, a clock skew correction to correct clock drift-induced error and a concurrent AoA system that is immune against TX scheduling uncertainty.

Bibliography

[1] Decawave. `https://www.decawave.com`. Accessed: 2020-05-04.

[2] Microsoft indoor localization competition - IPSN 2017. `https://www.microsoft.com/en-us/research/event/microsoft-indoor-localization-competition-ipsn-2017`. Accessed: 2020-05-04.

[3] Sources of error in DW1000-based two-way ranging (TWR) schemes. `https://www.decawave.com/sites/default/files/aps011_sources_of_error_in_twr.pdf`. Accessed: 2020-05-04.

[4] Ali-Rantala, P., Ukkonen, L., Sydanheimo, L., Keskilammi, M., and Kivikoski, M. Different kinds of walls and their effect on the attenuation of radiowaves indoors. In *IEEE Antennas and Propagation Society International Symposium. Digest. Held in conjunction with: USNC/CNC/URSI North American Radio Sci. Meeting (Cat. No. 03CH37450)* (2003), vol. 3, IEEE, pp. 1020–1023.

[5] Ansaripour, A., Heydariaan, M., Gnawali, O., and Kim, K. ViPER: Vehicle pose estimation using ultra-wideband radios. In *2020 16th International Conference on Distributed Computing in Sensor Systems (DCOSS)* (2020), IEEE.

[6] Corbalán, P., and Picco, G. P. Concurrent ranging in ultra-wideband radios: Experimental evidence, challenges, and opportunities. In *EWSN* (2018), pp. 55–66.

[7] Corbalán, P., Picco, G. P., and Palipana, S. Chorus: UWB concurrent transmissions for GPS-like passive localization of countless targets. In *2019 18th ACM/IEEE International Conference on Information Processing in Sensor Networks (IPSN)* (2019), IEEE, pp. 133–144.

[8] Decawave. *PDoA Primer - Calculating position directly from range and phase difference of arrival at two antennas*, 2018.

[9] Decawave. *DW1000*, 2020.

[10] Decawave. *DW1000 Datasheet*, 2020.

[11] Decawave. *DW1000 User Manual*, 2020.

[12] Decawave. *TREK1000 User Manual*, 2020.

[13] Di Franco, C., Prorok, A., Atanasov, N., Kempke, B., Dutta, P., Kumar, V., and Pappas, G. J. Calibration-free network localization using non-line-of-sight ultra-wideband measurements. In *2017 16th ACM/IEEE International Conference on Information Processing in Sensor Networks (IPSN)* (2017), IEEE, pp. 235–246.

[14] Dongare, A., Lazik, P., Rajagopal, N., and Rowe, A. Pulsar: A wireless propagation-aware clock synchronization platform. In *2017 IEEE Real-Time and Embedded Technology and Applications Symposium (RTAS)* (2017), IEEE, pp. 283–292.

[15] Dotlic, I., Connell, A., Ma, H., Clancy, J., and McLaughlin, M. Angle of arrival estimation using decawave DW1000 integrated circuits. In *2017 14th Workshop on Positioning, Navigation and Communications (WPNC)* (2017), IEEE, pp. 1–6.

[16] Eric, M., and Zetik, R. Non line of sight effects in UWB indoor direct one-step selflocalization using distributed antenna system: Measurement based study. In *WSA 2015; 19th International ITG Workshop on Smart Antennas* (2015), VDE, pp. 1–7.

[17] Falsi, C., Dardari, D., Mucchi, L., and Win, M. Z. Time of arrival estimation for UWB localizers in realistic environments. *EURASIP Journal on Advances in Signal Processing 2006*, 1 (2006), 032082.

[18] Ferrari, F., Zimmerling, M., Thiele, L., and Saukh, O. Efficient network flooding and time synchronization with Glossy. In *Proceedings of the 10th ACM/IEEE International Conference on Information Processing in Sensor Networks* (2011), IEEE, pp. 73–84.

[19] Gaffney, B. Combined LOS and NLOS UWB channel model. `https://www.decawave.com/wp-content/uploads/2018/12/Combined-LOS-and-NLOS-UWB-Channel-Model_2018-01-07.pdf`. Accessed: 2020-05-04.

[20] García, E., Poudereux, P., Hernández, Á., Ureña, J., and Gualda, D. A robust UWB indoor positioning system for highly complex environments. In *2015 IEEE International Conference on Industrial Technology (ICIT)* (2015), IEEE, pp. 3386–3391.

[21] Giri, D., and Tesche, F. Electromagnetic attenuation through various types of buildings. In *2013 Asia-Pacific Symposium on Electromagnetic Compatibility (APEMC)* (2013), IEEE, pp. 1–4.

[22] Großwindhager, B., Boano, C. A., Rath, M., and Römer, K. Concurrent ranging with ultra-wideband radios: From experimental evidence to a practical solution. In *2018 IEEE 38th International Conference on Distributed Computing Systems (ICDCS)* (2018), IEEE, pp. 1460–1467.

[23] Großwindhager, B., Stocker, M., Rath, M., Boano, C. A., and Römer, K. SnapLoc: an ultra-fast UWB-based indoor localization system for an unlimited number of tags. In *2019 18th ACM/IEEE International Conference on Information Processing in Sensor Networks (IPSN)* (2019), IEEE, pp. 61–72.

[24] Gururaj, K., Rajendra, A. K., Song, Y., Law, C. L., and Cai, G. Real-time identification of NLOS range measurements for enhanced uwb localization. In *2017 International Conference on Indoor Positioning and Indoor Navigation (IPIN)* (2017), IEEE, pp. 1–7.

[25] Heydariaan, M., Dabirian, H., and Gnawali, O. AnguLoc: Concurrent angle of arrival estimation for indoor localization with UWB radios. In *2020 16th International Conference on Distributed Computing in Sensor Systems (DCOSS)* (2020), IEEE.

[26] Heydariaan, M., Mohammadmoradi, H., and Gnawali, O. Toward standard non-line-of-sight benchmarking of ultra-wideband radio-based localization. In *2018 IEEE Workshop on Benchmarking Cyber-Physical Networks and Systems (CPSBench)* (2018), IEEE, pp. 19–24.

[27] Heydariaan, M., Mohammadmoradi, H., and Gnawali, O. R3: Reflection resilient concurrent ranging with ultra-wideband radios. In *2019 15th International Conference on Distributed Computing in Sensor Systems (DCOSS)* (2019), IEEE, pp. 1–8.

[28] Horváth, K. A., Ill, G., and Milánkovich, Á. Passive extended double-sided two-way ranging algorithm for UWB positioning. In *2017 Ninth International Conference on Ubiquitous and Future Networks (ICUFN)* (2017), IEEE, pp. 482–487.

[29] Humphrey, D., and Hedley, M. Super-resolution time of arrival for indoor localization. In *2008 IEEE International Conference on Communications* (2008), IEEE, pp. 3286–3290.

[30] IEEE. 802.15.4-2011 IEEE standard for local and metropolitan area networks-part 15.4: Low-rate wireless personal area networks (LR-WPANs). *IEEE Standards Association* (2011).

[31] Karanam, C. R., Korany, B., and Mostofi, Y. Magnitude-based angle-of-arrival estimation, localization, and target tracking. In *2018 17th ACM/IEEE International Conference on Information Processing in Sensor Networks (IPSN)* (2018), IEEE, pp. 254–265.

[32] Kempke, B., Pannuto, P., Campbell, B., and Dutta, P. SurePoint: Exploiting ultra wideband flooding and diversity to provide robust, scalable, high-fidelity indoor localization. In *Proceedings of the 14th ACM Conference on Embedded Network Sensor Systems CD-ROM* (2016), pp. 137–149.

[33] Kempke, B., Pannuto, P., and Dutta, P. Harmonium: Asymmetric, bandstitched uwb for fast, accurate, and robust indoor localization. In *2016 15th ACM/IEEE International Conference on Information Processing in Sensor Networks (IPSN)* (2016), IEEE, pp. 1–12.

[34] Kietlinski-Zaleski, J., and Yamazato, T. UWB positioning using known indoor features-environment comparison. In *2010 International Conference on Indoor Positioning and Indoor Navigation* (2010), IEEE, pp. 1–9.

[35] Kim, H., Ma, X., and Hamilton, B. R. Tracking low-precision clocks with time-varying drifts using Kalman filtering. *IEEE/ACM Transactions on Networking (TON) 20*, 1 (2012), 257–270.

[36] Kolakowski, M., and Djaja-Josko, V. TDOA-TWR based positioning algorithm for uwb localization system. In *2016 21st International Conference on Microwave, Radar and Wireless Communications (MIKON)* (2016), IEEE, pp. 1–4.

[37] Lemic, F. Service for calculation of performance metrics of indoor localization benchmarking experiments. *Telecommunication Networks Group, Tech. Rep. TKN-14-003* (2014).

[38] Li, C., Li, H.-B., and Kohno, R. Performance evaluation of IEEE 802.15.4 for wireless body area network (WBAN). In *2009 IEEE International conference on communications workshops* (2009), IEEE, pp. 1–5.

[39] Lueth, K. L. State of the IoT 2018: Number of IoT devices now at 7b - market accelerating. `https://iot-analytics.com/state-of-the-iot-update-q1-q2-2018-number-of-iot-devices-now-7b/`. Accessed: 2020-03-30.

[40] Luong, A., Hillyard, P., Abrar, A., Che, C., Rowe, A., Schmid, T., and Patwari, N. A stitch in time and frequency synchronization saves bandwidth. In *2018 17th ACM/IEEE International Conference on Information Processing in Sensor Networks (IPSN)* (2018), IEEE, pp. 96–107.

[41] Marano, S., Gifford, W. M., Wymeersch, H., and Win, M. Z. NLOS identification and mitigation for localization based on uwb experimental data. *IEEE Journal on selected areas in communications 28*, 7 (2010), 1026–1035.

[42] Maróti, M., Kusy, B., Simon, G., and Lédeczi, Á. The flooding time synchronization protocol. In *Proceedings of the 2nd international conference on Embedded networked sensor systems* (2004), pp. 39–49.

[43] Mazhar, F., Khan, M. G., and Sällberg, B. Precise indoor positioning using UWB: a review of methods, algorithms and implementations. *Wireless Personal Communications 97*, 3 (2017), 4467–4491.

[44] McLaughlin, M., McElroy, C., Wilmot, S., and Proudfoot, T. Receiver for use in an ultra-wideband communication system, June 24 2014. US Patent 8,760,334.

[45] McLaughlin, M., Neirynck, D., and McElroy, C. Timing recovery for use in an ultra-wideband communication system, Nov. 26 2019. US Patent 10,491,266.

[46] McLaughlin, M., and Verso, B. Asymmetric double-sided two-way ranging in an ultrawideband communication system, Nov. 26 2019. US Patent 10,488,509.

[47] Micheli, D., Delfini, A., Santoni, F., Volpini, F., and Marchetti, M. Measurement of electromagnetic field attenuation by building walls in the mobile phone and satellite navigation frequency bands. *IEEE Antennas and Wireless Propagation Letters 14* (2015), 698–702.

[48] Mohammadmoradi, H., and Gnawali, O. Study and mitigation of non-cooperative UWB interference on ranging. In *EWSN* (2019), pp. 142–153.

[49] Mohammadmoradi, H., Heydariaan, M., and Gnawali, O. UWB physical layer adaptation for best ranging performance within application constraints. In *Proceedings of the 2nd International Conference on Smart Digital Environment* (2018), pp. 119–126.

[50] Mohammadmoradi, H., Heydariaan, M., and Gnawali, O. SRAC: Simultaneous ranging and communication in UWB networks. In *2019 15th International Conference on Distributed Computing in Sensor Systems (DCOSS)* (2019), IEEE, pp. 9–16.

[51] Mohammadmoradi, H., Heydariaan, M., Gnawali, O., and Kim, K. UWB-based single-anchor indoor localization using reflected multipath components. In *2019 International Conference on Computing, Networking and Communications (ICNC)* (2019), IEEE, pp. 308–312.

[52] Neirynck, D., O'Duinn, M., and McElroy, C. Characterisation of the NLOS performance of an IEEE 802.15.4a receiver. In *12th Workshop on Navigation, Positioning and Communications (WPNC)* (2015).

[53] Noh, K.-L., Chaudhari, Q. M., Serpedin, E., and Suter, B. W. Novel clock phase offset and skew estimation using two-way timing message exchanges for wireless sensor networks. *IEEE transactions on communications 55*, 4 (2007), 766–777.

[54] Rout, D. K., and Das, S. Multiple narrowband interference mitigation using hybrid hermite pulses for body surface to external communications in UWB body area networks. *Wireless Networks 23*, 2 (2017), 387–402.

[55] Sahinoglu, Z., and Gezici, S. Ranging in the IEEE 802.15.4a standard. In *2006 IEEE Annual Wireless and Microwave Technology Conference* (2006), IEEE, pp. 1–5.

[56] Santos, E. R., Azpurua, H., Rezeck, P. A., Corrêa, M. F., Vieira, M. A., Freitas, G. M., and Macharet, D. G. Localization using ultra wideband and IEEE 802.15.4 radios with nonlinear bayesian filters: a comparative study. *Journal of Intelligent & Robotic Systems* (2020), 1–17.

[57] Shanno, D. F. Conditioning of quasi-Newton methods for function minimization. *Mathematics of computation 24*, 111 (1970), 647–656.

[58] Shao, H.-J., Zhang, X.-P., and Wang, Z. Efficient closed-form algorithms for AOA based self-localization of sensor nodes using auxiliary variables. *IEEE Transactions on Signal Processing 62*, 10 (2014), 2580–2594.

[59] Silva, B., Dos Santos, R., and Hancke, G. P. Towards non-line-of-sight ranging error mitigation in industrial wireless sensor networks. In *IECON 2016-42nd Annual Conference of the IEEE Industrial Electronics Society* (2016), IEEE, pp. 5687–5692.

[60] Silva, B., and Hancke, G. Characterization of non-line of sight paths using 802.15.4a. In *2017 IEEE International Conference on Industrial Technology (ICIT)* (2017), IEEE, pp. 1436–1440.

[61] Stolhofer, D., Doelecke, H., Liu, Y., and O'eary, P. RF propagation through transparent conductors in energy efficient windows. In *2010 European Wireless Conference (EW)* (2010), IEEE, pp. 177–181.

[62] Stone, W. C. NIST construction automation program report no. 3: Electromagnetic signal attenuation in construction materials (NISTIR 6055). *National Technical Information Service, Washington (October 1997)* (1997).

[63] Taylor, C. D., Gutierrez, S. J., Langdon, S. L., and Murphy, K. On the propagation of RF into a building constructed of cinder block over the frequency range 200 MHz to 3 GHz. *IEEE transactions on electromagnetic compatibility 41*, 1 (1999), 46–49.

[64] Tian, Z., Li, Y., Zhou, M., and Lian, Y. WLAN indoor localization using angle of arrival. In *International Conference on Machine Learning and Intelligent Communications* (2017), Springer, pp. 112–121.

[65] Vecchia, D., Corbalán, P., Istomin, T., and Picco, G. P. Playing with fire: Exploring concurrent transmissions in ultra-wideband radios. In *2019 16th Annual IEEE International Conference on Sensing, Communication, and Networking (SECON)* (2019), IEEE, pp. 1–9.

[66] Wang, T., Zhao, H., and Shen, Y. An efficient single-anchor localization method using ultra-wide bandwidth systems. *Applied Sciences 10*, 1 (2020), 57.

[67] Wielandt, S., and Strycker, L. D. Indoor multipath assisted angle of arrival localization. *Sensors 17*, 11 (2017), 2522.

[68] Yildirim, K. S., and Kantarci, A. Time synchronization based on slow-flooding in wireless sensor networks. *IEEE Transactions on Parallel and Distributed Systems 25*, 1 (2014), 244–253.

[69] Yu, K., Wen, K., Li, Y., Zhang, S., and Zhang, K. A novel NLOS mitigation algorithm for UWB localization in harsh indoor environments. *IEEE Transactions on Vehicular Technology 68*, 1 (2018), 686–699.

[70] Zhang, Y., Brown, A. K., Malik, W. Q., and Edwards, D. J. High resolution 3-D angle of arrival determination for indoor UWB multipath propagation. *IEEE Transactions on Wireless Communications 7*, 8 (2008), 3047–3055.

[71] Zhu, B., Cheng, J., Wang, Y., Yan, J., and Wang, J. Three-dimensional VLC positioning based on angle difference of arrival with arbitrary tilting angle of receiver. *IEEE Journal on Selected Areas in Communications 36*, 1 (2017), 8–22.